The Supplementary Information for

Amide Cyclodextrin That Recognises Monophosphate Anions in Harmony with Water Molecules

Takashi Nakamura*[a], Hayato Takayanagi[b], Masaki Nakahata*[c], Takumi Okubayashi[d], Hitomi Baba[e], Yoshiki Ishii[f], Go Watanabe*[e,f,g], Daisuke Tanabe[d], and Tatsuya Nabeshima[a]

[a]Institute of Pure and Applied Sciences, University of Tsukuba, 1-1-1 Tennodai, Tsukuba, Ibaraki 305-8571, Japan
[b]Degree Programs in Pure and Applied Sciences, Graduate School of Science and Technology, University of Tsukuba, 1-1-1 Tennodai, Tsukuba, Ibaraki 305-8571, Japan
[c]Graduate School of Science, Osaka University, 1-1 Machikaneyama-cho, Toyonaka, Osaka 560-0043, Japan
[d]School of Science and Engineering, University of Tsukuba, 1-1-1 Tennodai, Tsukuba, Ibaraki 305-8571, Japan
[e]School of Science, Kitasato University, 1-15-1 Kitazato, Minami-ku, Sagamihara, Kanagawa 252-0373, Japan
[f]School of Frontier Engineering, Kitasato University, 1-15-1 Kitazato, Minami-ku, Sagamihara, Kanagawa 252-0373, Japan
[g]Kanagawa Institute of Industrial Science and Technology, 705-1 Shimoimaizumi, Ebina, Kanagawa 243-0435, Japan

*Corresponding Authors. Email: nakamura@chem.tsukuba.ac.jp (Takashi Nakamura)

nakahata@chem.sci.osaka-u.ac.jp (Masaki Nakahata)

go0325@kitasato-u.ac.jp (Go Watanabe)

Table of Contents

1. Materials and methods S3
2. Synthesis of amide cyclodextrin derivatives S4
3. Characterization of amide cyclodextrin derivatives S6
4. NMR and UV studies of anion recognition S16
5. Isothermal titration calorimetry S43
6. Molecular modeling and simulation S45
7. References for the supplementary information S52

1. Materials and methods

Unless otherwise noted, solvents and reagents were purchased from Tokyo Chemical Industry Co., Ltd., Fujifilm Wako Pure Chemical Corporation, Kanto Chemical Co., Inc., Kishida Chemical Co., Ltd., Nacalai Tesque, Inc., Sigma-Aldrich or Dojindo Laboratories and used without further purification. Dry THF and DMF were purified by Glass Contour Ultimate Solvent System. Automated flash chromatography purifications were performed using a Biotage Isolera One system with Biotage Sfär Silica (HC D 20 μm) columns. Ion exchange column chromatography was performed using DOWEX 50Wx8 50-100 Mesh (H) Cation Exchange Resin. Size-exclusion chromatography was performed using Sephadex G-10.

Measurements were performed at 298 K unless otherwise noted. ^{1}H, ^{13}C, ^{19}F, ^{31}P NMR, and other 2D NMR spectra were recorded on Bruker AVANCE III-400 and 600 spectrometers. Negative values were depicted in red in the spectra. Tetramethylsilane was used as an internal standard (δ 0.00 ppm) for ^{1}H and ^{13}C NMR measurements when $CDCl_3$ or DMSO-d_6 was used as solvents. Solvent residual signals were used as a standard for ^{1}H and ^{13}C NMR measurements when solvents other than $CDCl_3$ or DMSO-d_6 were used[S1]. Hexafluorobenzene in $CDCl_3$ (1 wt %) was used as an external standard (δ –163.0 ppm) for ^{19}F NMR measurements. 80% Phosphoric acid aqueous solution was used as an external standard (δ 0.00 ppm) for ^{31}P NMR measurements. The assignments of the ^{1}H and ^{13}C signals were based on ^{1}H-^{1}H COSY, ^{1}H-^{1}H NOESY (or ^{1}H-^{1}H ROESY), ^{1}H-^{13}C HSQC, and ^{1}H-^{13}C HMBC experiments.

MALDI TOF mass data were recorded on an AB SCIEX TOF/TOF 5800 system. ESI-TOF mass data were recorded on an AB SCIEX TripleTOF 4600 system. UV-Vis spectra were recorded on a JASCO V-670 spectrophotometer. Circular dichroism spectra were recorded on a JASCO J-820 spectrophotometer. IR spectra were recorded on a JASCO FT/IR-480 Fourier transform infrared spectrometer. Melting point was measured by a Yanaco MP-J3 melting point apparatus.

Elemental analysis was performed on a Yanaco MT-6 analyzer with tin boats purchased from Elementar. We appreciate Mr. Masao Sasaki for the measurements.

Isothermal titration calorimetry (ITC) measurements were carried out using a MicroCal PEAQ-ITC (Malvern Panalytical, Malvern, UK). ITC experiments to determine the thermodynamic parameters were performed three times.

DFT calculations were implemented with Gaussian 16[S2] to determine the atomic charges of host and guest molecules used in a force field, and MD calculations were implemented with Gromacs 2016.6[S3] to compute the host-guest interaction. The computer resources were provided by the Research Center for Computational Science in Okazaki, Grand Chariot at Hokkaido University, and OCTOPUS at Osaka University were utilized here partially through the HPCI System Research Project.

We appreciate the Open Facility Network Office, Research Facility Center for Science and Technology, University of Tsukuba, for MALDI TOF mass measurements.

2. Synthesis of amide cyclodextrin derivatives

Synthesis of **2**

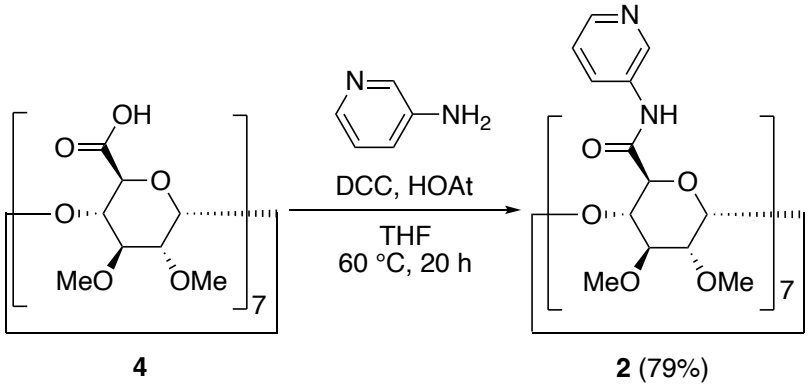

4 **2** (79%)

Scheme S1. Synthesis of **2**

4[S4] (601 mg, 0.420 mmol, 1.0 equiv) and 1-hydroxy-7-azabenzotriazole (629 mg, 4.62 mmol, 11 equiv) were added to a 100 mL eggplant flask, and the atmosphere was replaced with argon. Dicyclohexylcarbodiimide (1.908 g, 9.25 mmol, 22 equiv) and dry THF (14 mL) were added to the flask, and the mixture was stirred at 60 °C. Then, THF solution (18 mL) of 3-aminopyridine (2.531 g, 26.9 mmol, 64 equiv) was added via cannulation, and the mixture was stirred at 60 °C for 20 h. MeOH (12 mL) was added to the flask and the mixture was concentrated in vacuo. 1 M HCl aq (34 mL) was added to the residue, and the remaining solid was removed by filtration. 1 M $NaHCO_3$ aq (30 mL) was added to the filtrate, then the aqueous layer (pH 8–9) was transferred to a separating funnel and extracted with $CHCl_3$ (50 mL × 4). The combined organic layer was dried over Na_2SO_4, filtered, and concentrated in vacuo. The residue was purified by flash column chromatography (eluent: AcOEt/MeOH/Et_2NH = 100/0/1−50/50/1). The obtained fractions were concentrated in vacuo. $CHCl_3$ (100 mL) was added to the residue, then the organic layer was transferred to a separating funnel and washed with 1 M $NaHCO_3$ aq (100 mL) to remove $Et_2NH_2^+$ salt. The organic layer was dried over Na_2SO_4, filtered, and concentrated in vacuo to give **2** (650 mg, 0.331 mmol, 79%).

Pale pink solid; m.p. 211.0–212.0 °C;

^{1}H NMR ($CDCl_3$, 600 MHz): δ 9.41 (br, 7H), 8.47 (s, 7H), 8.08 (d, J = 4.2 Hz, 7H), 7.57 (br, 7H), 6.84 (br, 7H), 5.33 (br, 7H), 4.63 (d, J = 7.2 Hz, 7H), 4.10 (br, 7H), 3.77 (dd, J = 7.5, 7.5 Hz, 7H), 3.62 (s, 21H), 3.56 (s, 21H), 3.32 (br, 7H);

^{13}C NMR ($CDCl_3$, 151 MHz): δ 168.1, 145.6, 142.7, 133.8, 128.3, 123.3, 99.0, 80.7, 80.2, 79.5(br), 72.6, 60.4, 58.6;

MALDI-TOF-MS: *m/z* $[M+Na]^+$ calcd. for $C_{91}H_{112}N_{14}O_{35}Na$, 1984.7; found 1984.7;

HRMS (ESI): *m/z* $[M+2H]^{3+}$ calcd. for $C_{91}H_{115}N_{14}O_{35}$ 654.5883, found 654.5862;

IR (KBr) ν_{max}: 1685 (s, C=O), 3283 cm^{-1};

Elemental analysis: calcd. for $C_{59}H_{134}N_{14}O_{42.5}$ (**2**· $7.5H_2O$·$0.5C_6H_{14}$) C, 52.75; H, 6.31; N, 9.16. found: C, 52.53; H, 6.01; N, 9.28. (The sample for elemental analysis was purified by reprecipitation ($CHCl_3$/*n*-hexane).)

Synthesis of **1**$(OTf)_7$

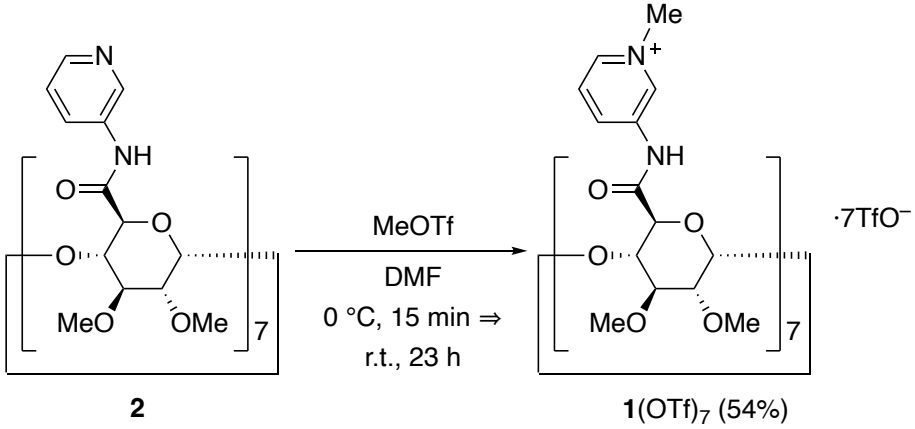

Scheme S2. Synthesis of **1**$(OTf)_7$

2 (150.1 mg, 76.5 μmol, 1.0 equiv) was added to a 10 mL pear-shaped flask, and the atmosphere was replaced with argon. Dry DMF (0.60 mL) was added to the flask, and the solution was stirred at 0 °C. Then, methyl trifluoromethanesulfonate (0.585 mL, 5.35 mmol, 70 equiv) was added to the flask, and the mixture was stirred at 0 °C for 15 min and at room temperature for 23 h. Then, MeOH (3 mL) was added to the flask and the mixture was concentrated in vacuo. The residue was purified by size-exclusion chromatography (Sephadex G-10, eluent: H_2O). The obtained fractions were purified by reprecipitation (EtOH/Et_2O) to give **1**$(OTf)_7$ (128.1 mg, 41.2 μmol, 54%).

Colorless solid; m.p. 160 °C (decomp.);

^{1}H NMR (CD_3OD, 600 MHz): δ 9.21 (s, 7H), 8.43 (d, J = 3.6 Hz, 7H), 8.41 (br, 7H), 7.75 (br, 7H), 5.29 (s, 7H), 4.53 (d, J = 7.2 Hz, 7H), 4.28 (s, 21H), 3.95 (dd, J = 7.2, 7.8 Hz, 7H), 3.75 (br, 7H), 3.71 (s, 21H), 3.55 (s, 21H), 3.38 (br, 7H);

^{13}C NMR (CD_3OD, 151 MHz): δ 170.8, 141.7, 140.0, 137.7, 135.6, 129.2, 121.8 (CF_3SO_3, q, $J_{C\text{-}F}$ = 318.8 Hz), 99.9, 82.7, 82.3, 82.2, 75.1, 61.7, 59.3, 49.7;

^{19}F NMR (CD_3OD, 565 MHz) δ –79.9;

HRMS (ESI): *m/z* $[M+3TfO–H]^{3+}$ calcd. for $C_{101}H_{132}N_{14}O_{44}S_3F_9$ 837.2513, found 837.2508;

IR (KBr) ν_{max}: 1710 (s, C=O), 3097, 3279, 3502 cm^{-1};

Elemental analysis: calcd. for $C_{105}H_{143}N_{14}O_{61}S_7F_{21}$ (**1**$(OTf)_7 \cdot 5H_2O$) C, 39.40; H, 4.50; N, 6.13. found: C, 39.49; H, 4.48; N, 5.85.

3. Characterization of amide cyclodextrin derivatives

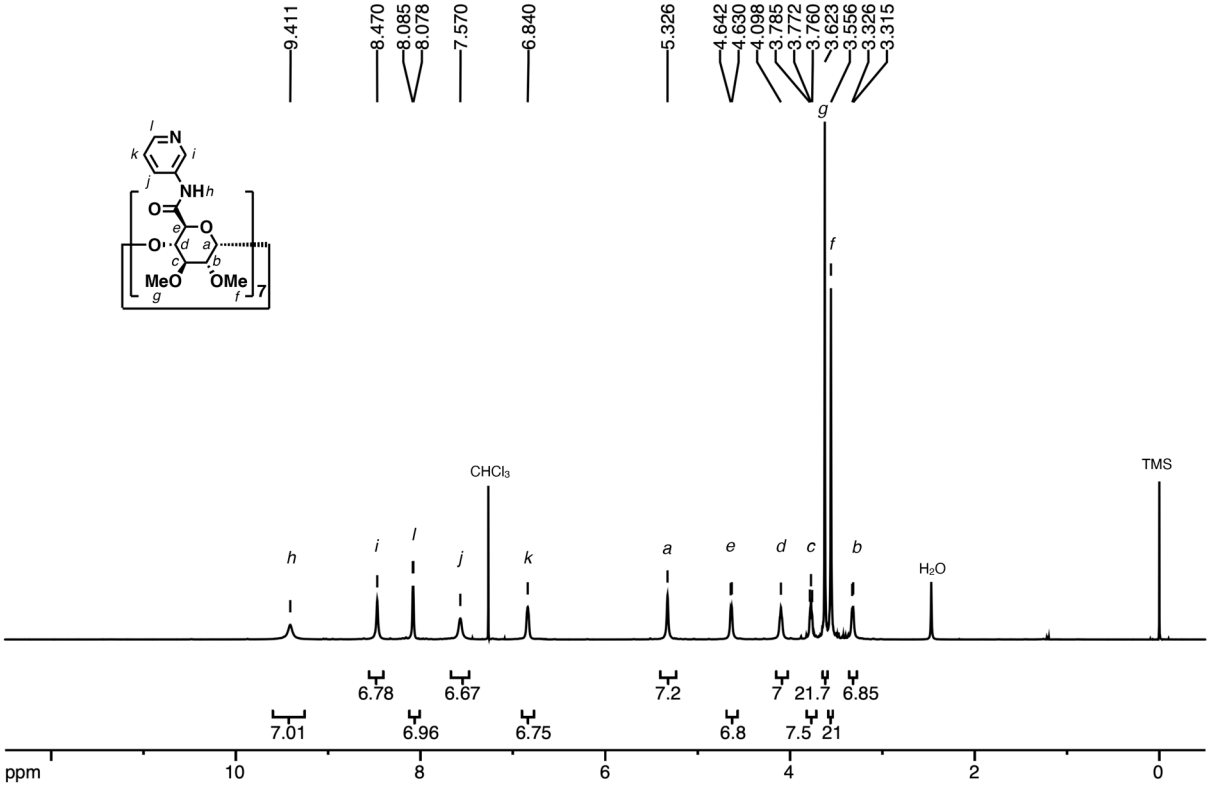

Figure S1. ^{1}H NMR spectrum of **2** ($CDCl_3$, 600 MHz)

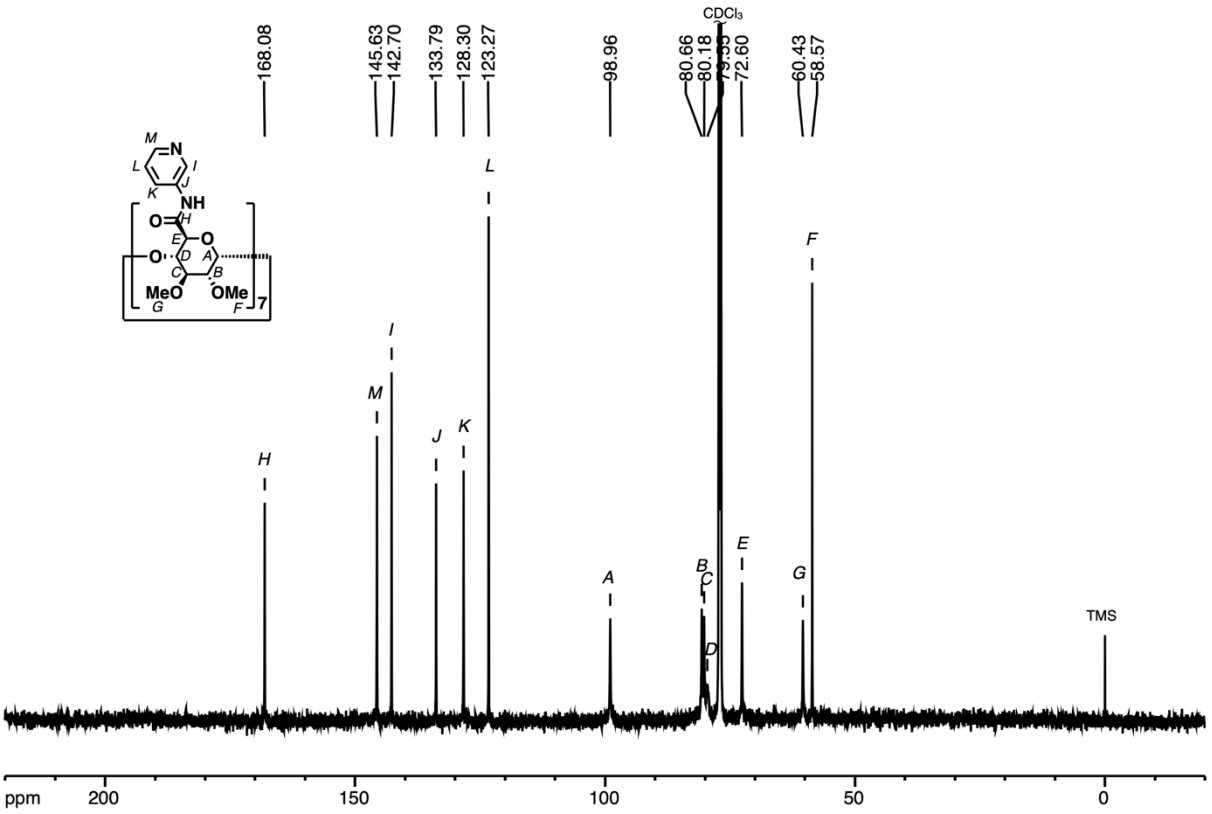

Figure S2. ^{13}C NMR spectrum of **2** ($CDCl_3$, 151 MHz)

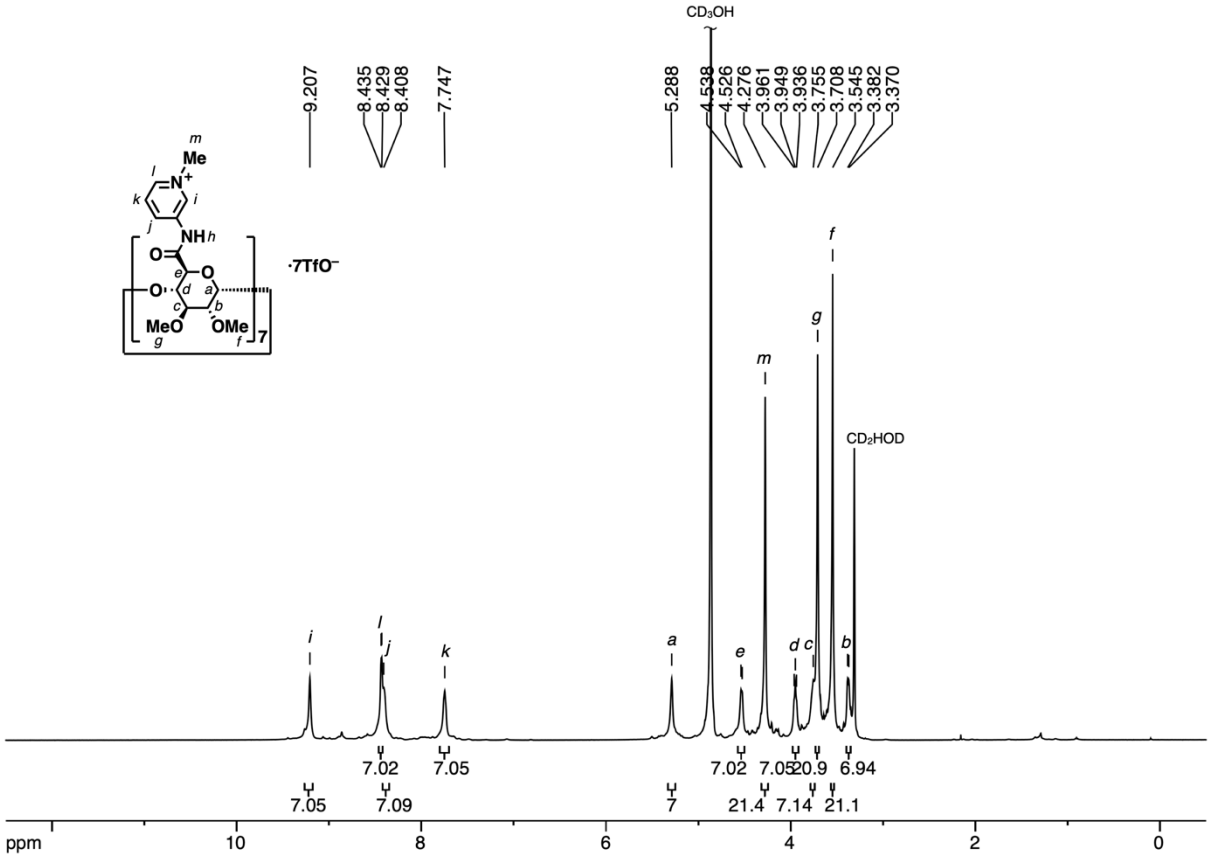

Figure S3. ^{1}H NMR spectrum of **1**(OTf)$_7$ (CD_3OD, 600 MHz). Appearance of the small signals are dependent on the solvents (Fig. S13), and the signals are considered to be those of a conformational isomer of **1**(OTf)$_7$, such as a self-inclusion complex[S5,S6].

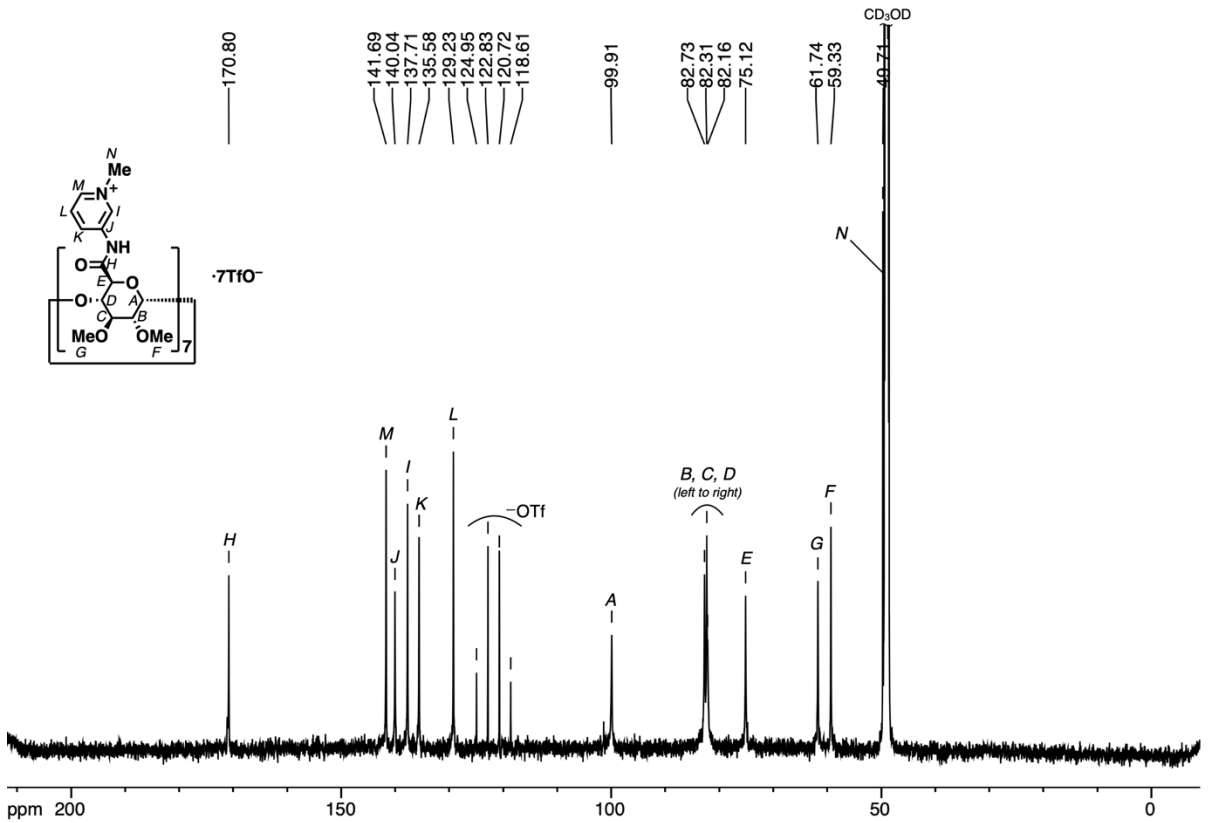

Figure S4. ^{13}C NMR spectrum of **1**(OTf)$_7$ (CD_3OD, 151 MHz).

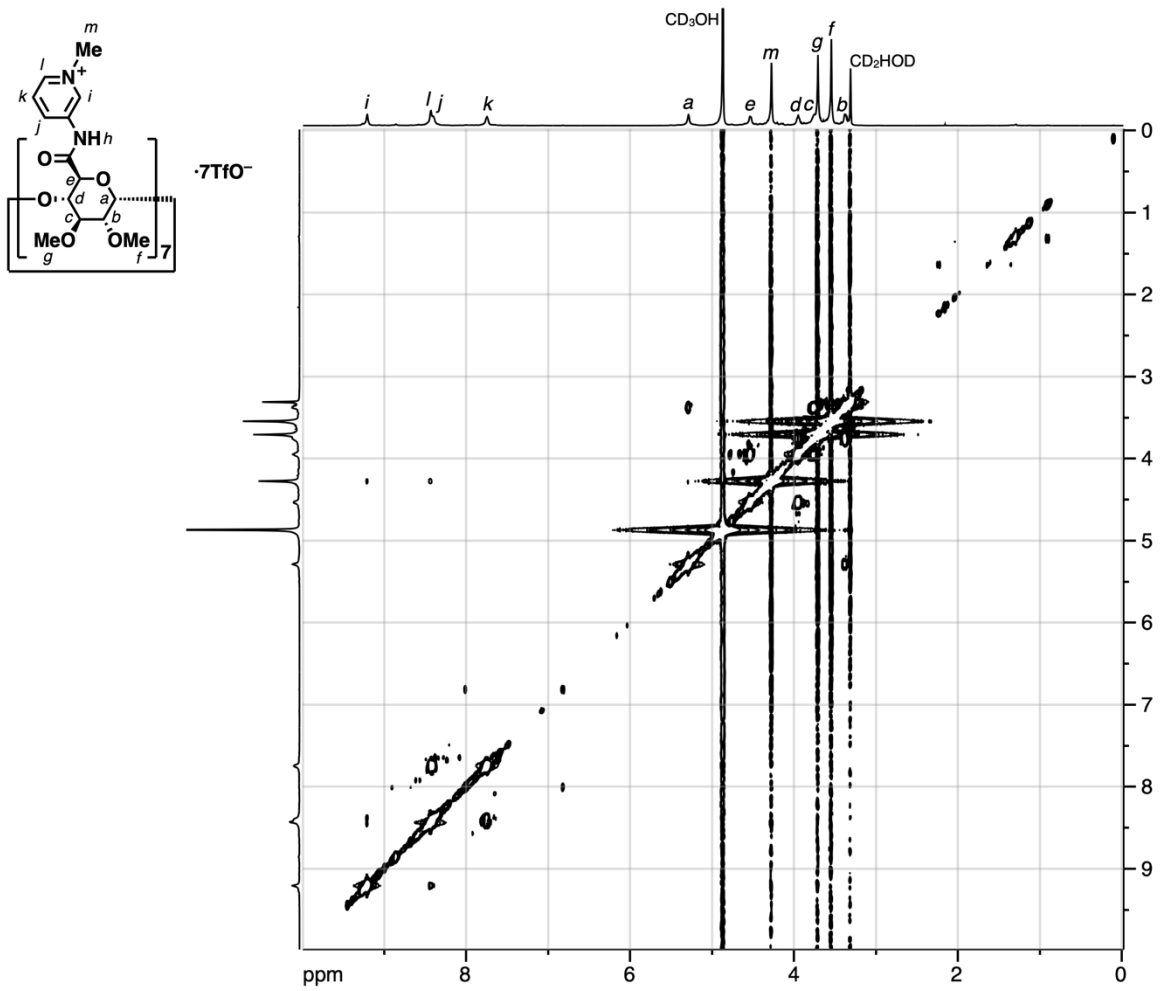

Figure S5. ^{1}H–^{1}H COSY spectrum of **1**(OTf)$_7$ (CD_3OD, 600 MHz).

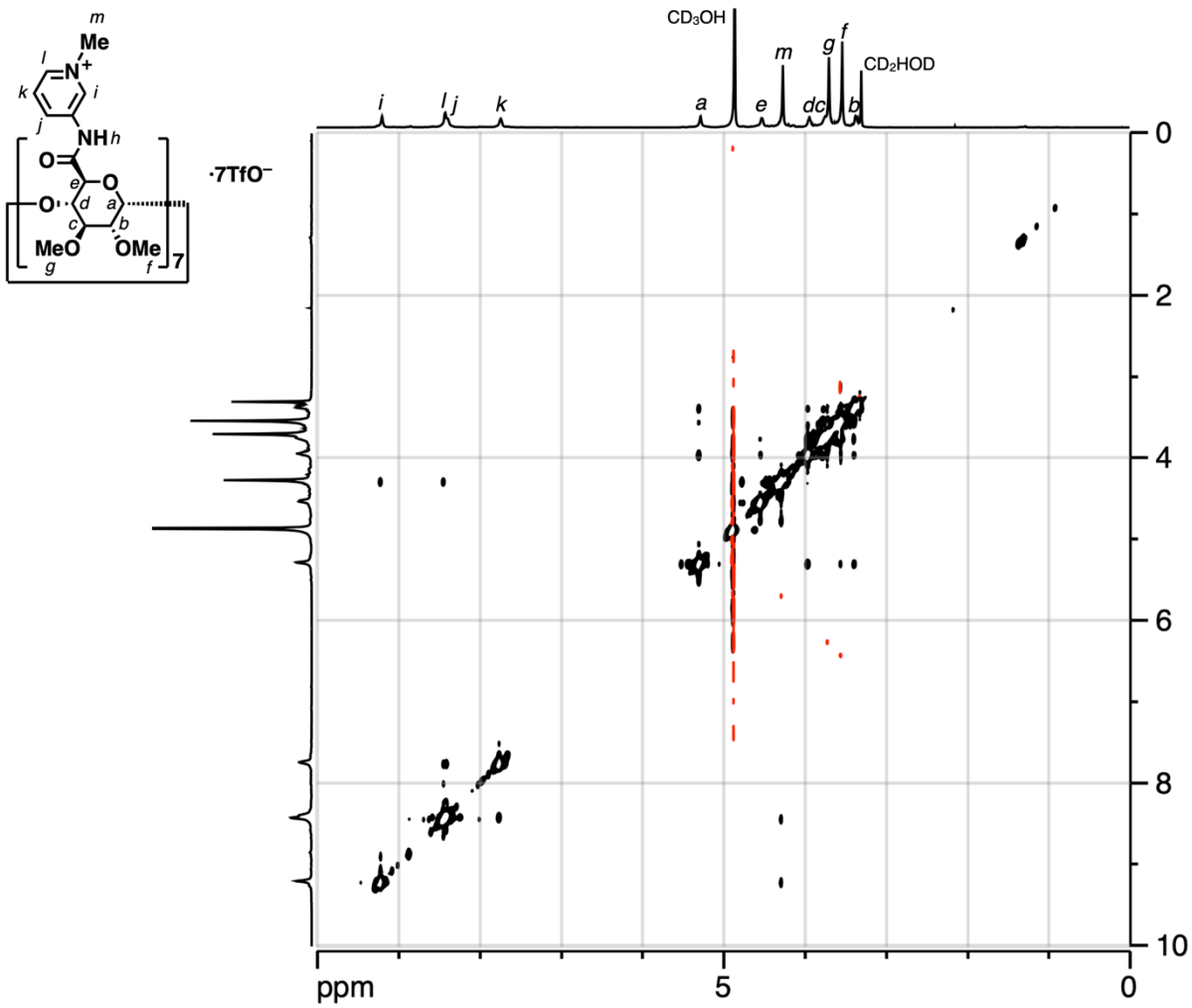

Figure S6. ^{1}H–^{1}H NOESY spectrum of **1**(OTf)$_7$ (CD_3OD, 600 MHz).

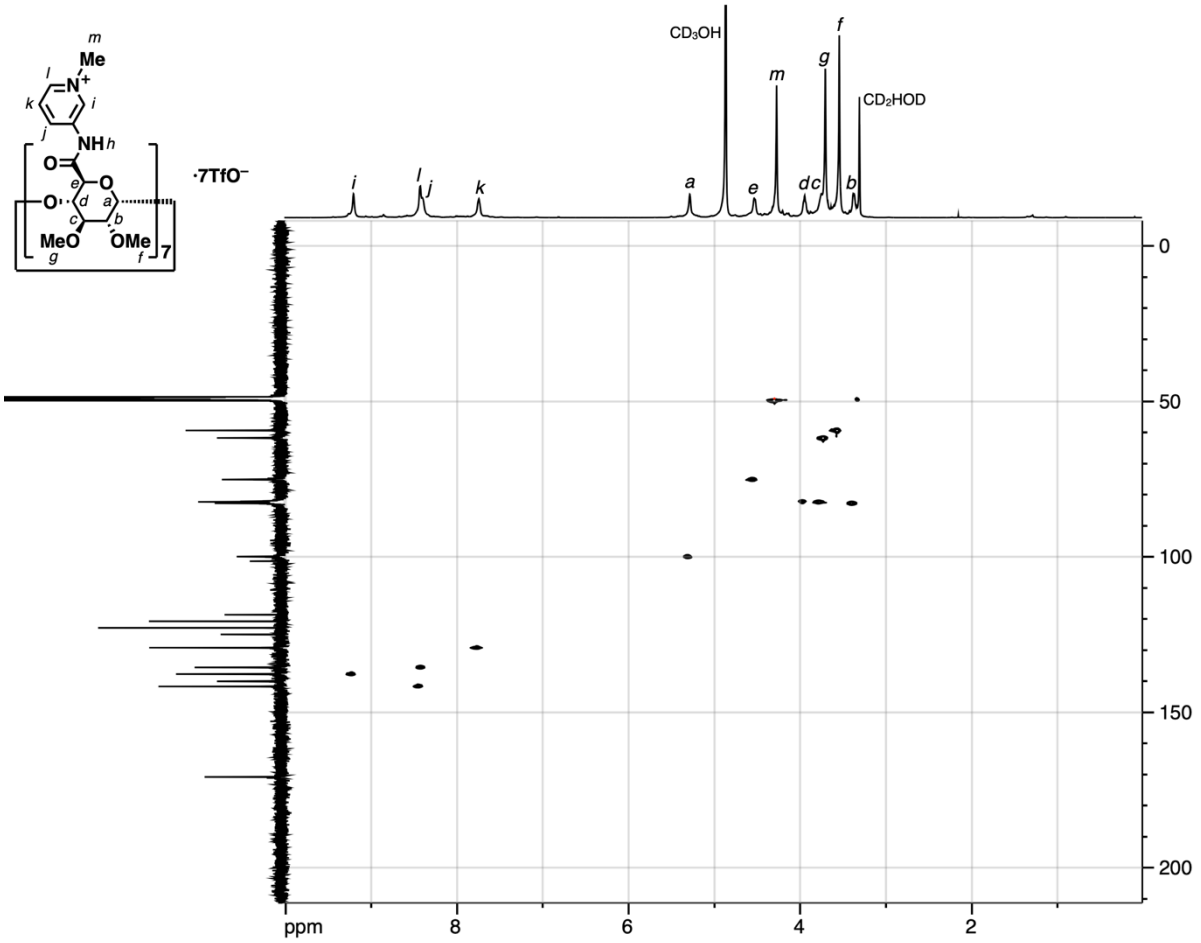

Figure S7. ^{1}H–^{13}C HSQC spectrum of **1**$(OTf)_7$ (CD_3OD, 600 MHz).

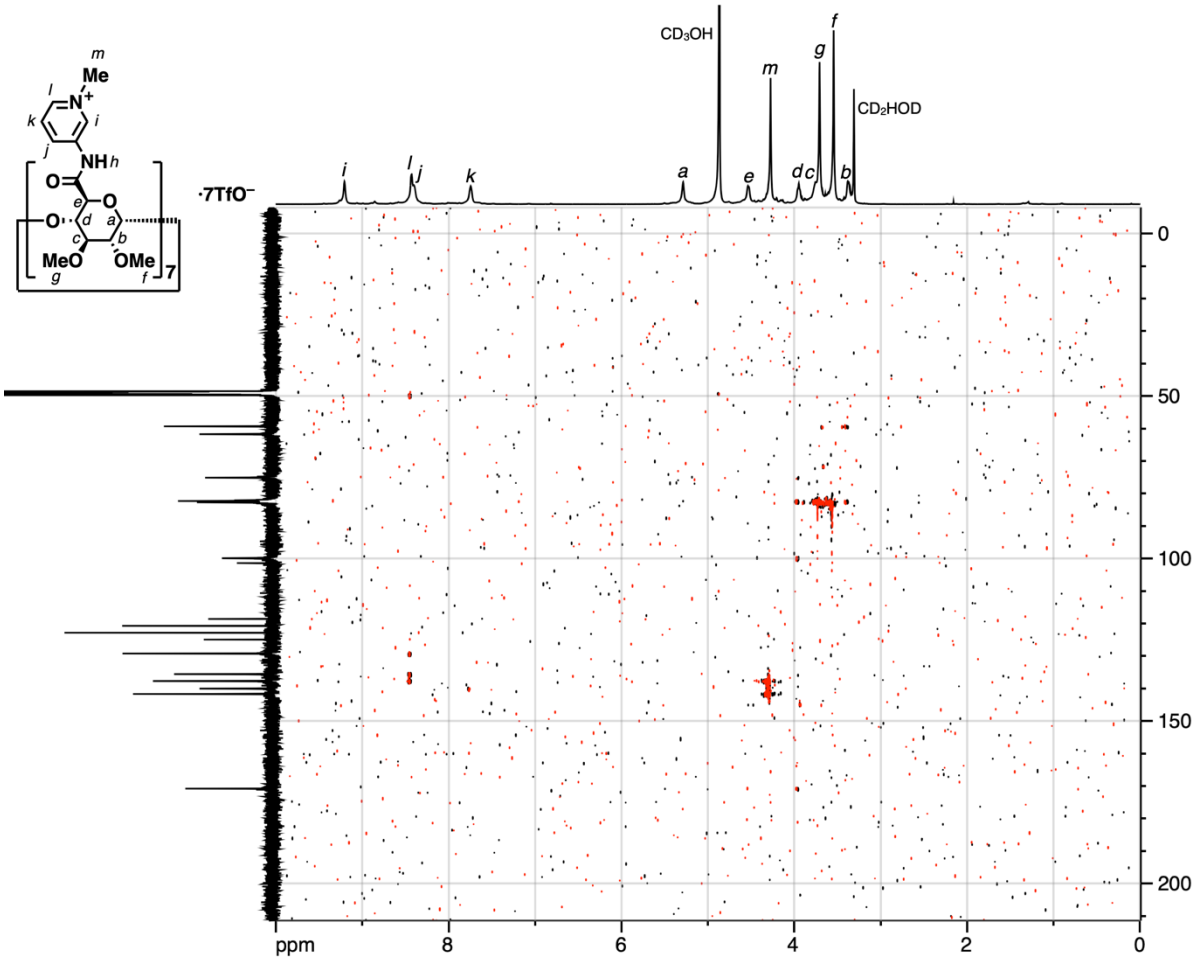

Figure S8. $^{1}H–^{13}C$ HMBC spectrum of **1**$(OTf)_7$ (CD_3OD, 600 MHz).

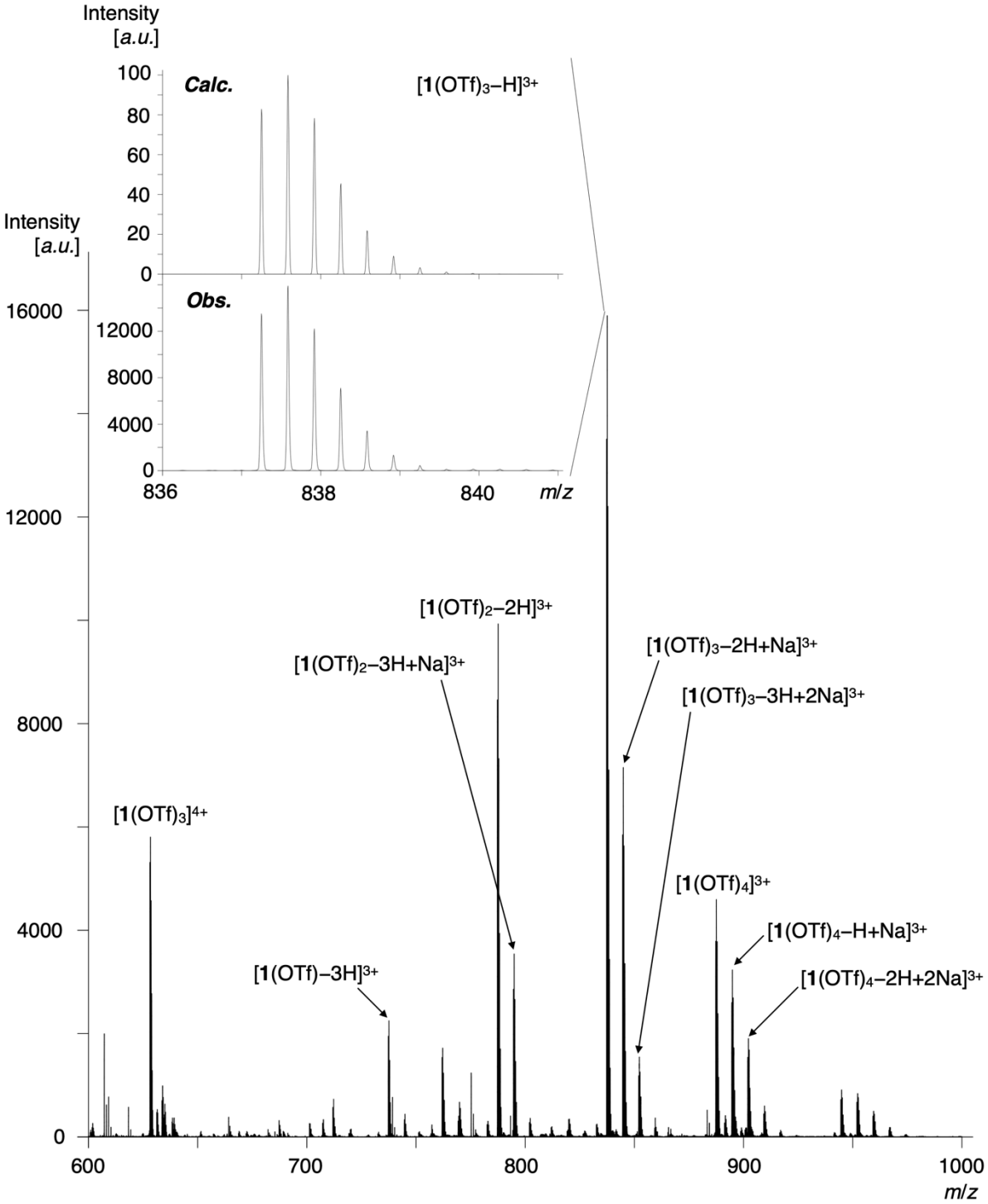

Figure S9. ESI-TOF mass spectrum of **1**$(OTf)_7$ (positive, MeOH).

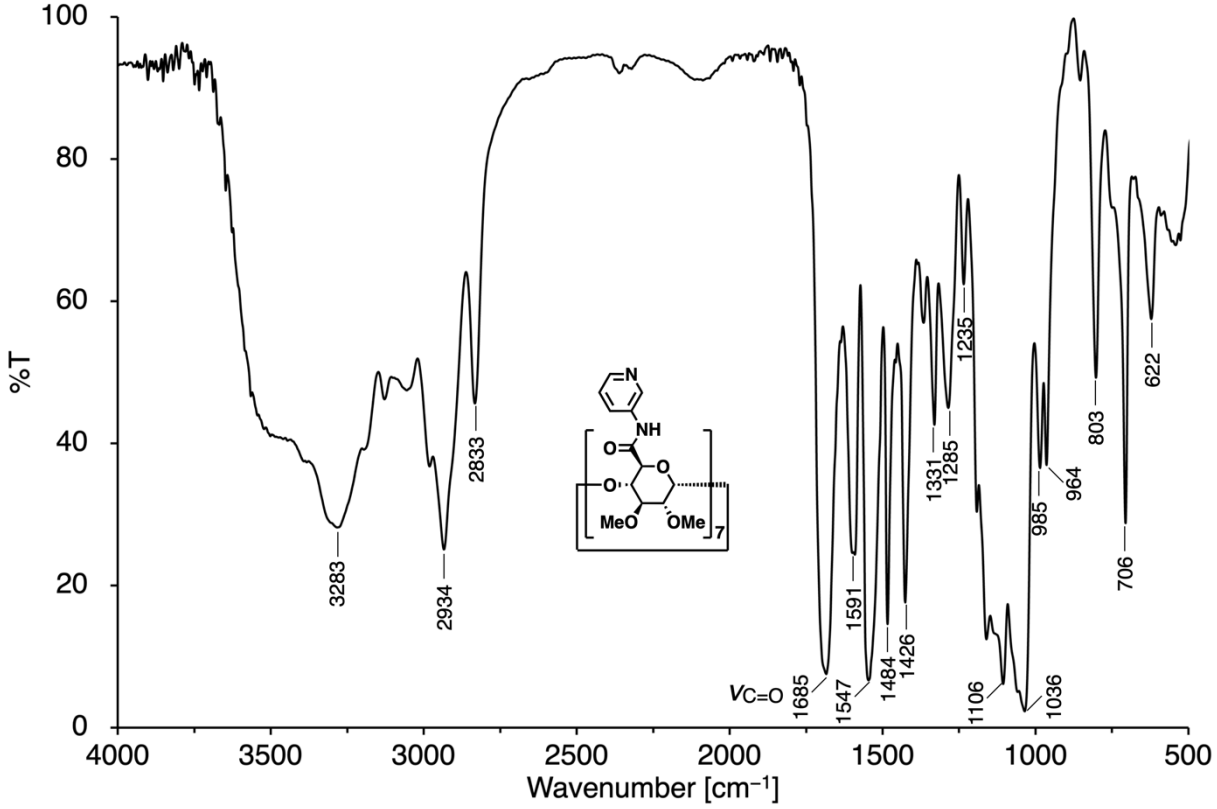

Figure S10. IR spectrum of **2** (KBr).

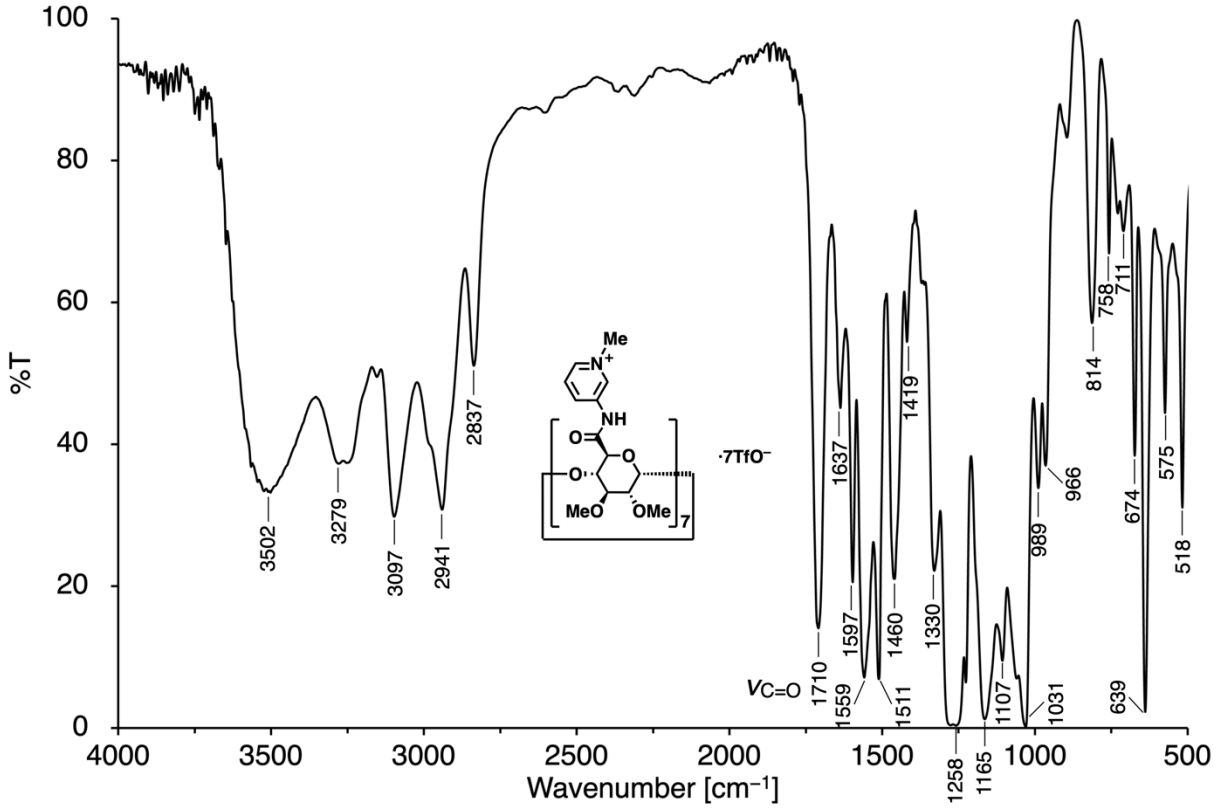

Figure S11. IR spectrum of **1**$(OTf)_7$ (KBr).

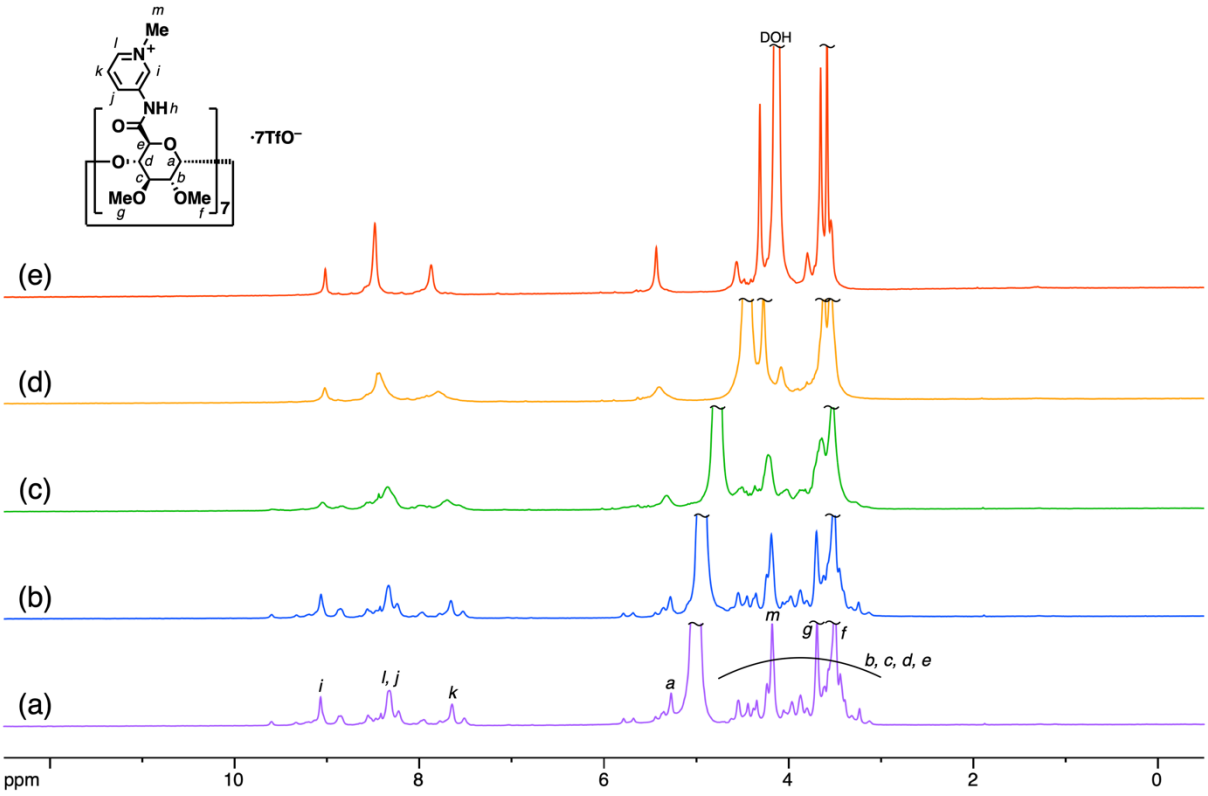

Figure S12. ^{1}H NMR spectra of **1**(OTf)$_7$ at various temperatures (D_2O, 600 MHz). (a) 278 K. (b) 283 K. (c) 298 K. (d) 328 K. (e) 363 K.

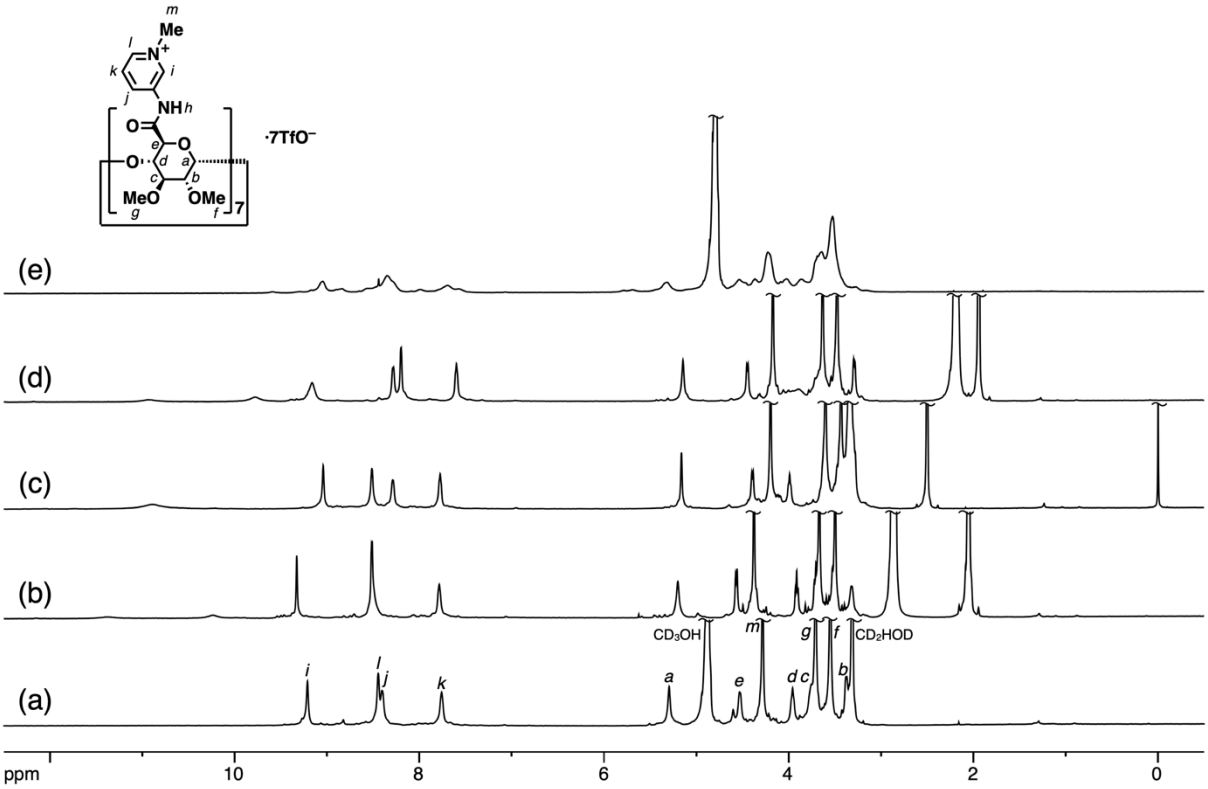

Figure S13. ^{1}H NMR spectra of **1**(OTf)$_7$ in various solvents (600 MHz). (a) CD_3OD. (b) Acetone-d_6. (c) DMSO-d_6. (d) CD_3CN. (e) D_2O.

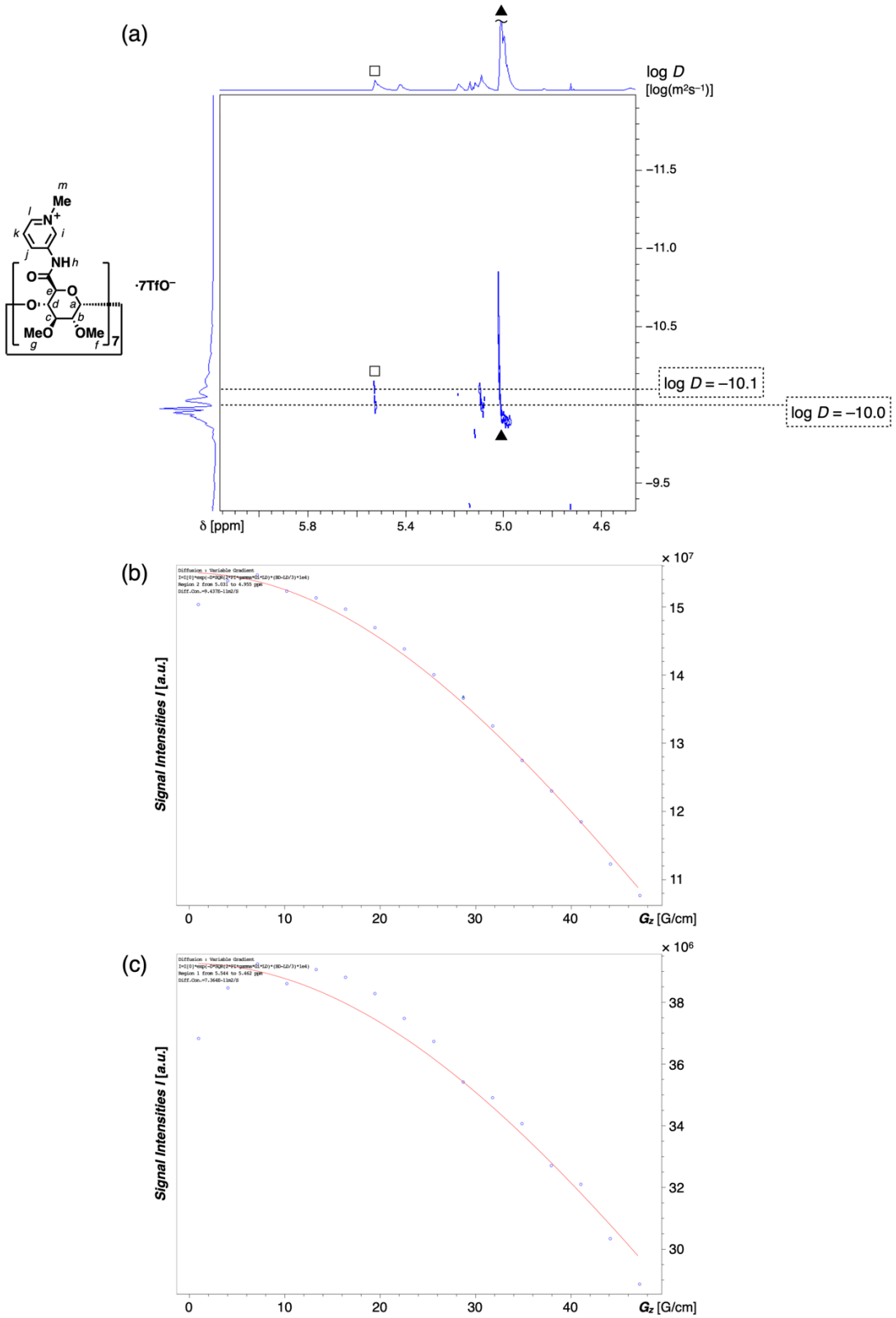

Figure S14. (a) ^{1}H DOSY spectrum of **1**(OTf)$_7$ (278 K, D_2O, 600 MHz). (b) A curve fitting of signal ▲ (C_7 isomer) to determine the diffusion constant D [m^2s^{-1}]. (c) A curve fitting of signal □ (C_1 isomer) to determine the diffusion constant D.

The diffusion constants of **1**(OTf)$_7$ were log$D$ = –10.1 for C_7 isomer, and log$D$ = –10.0 for C_1 isomer, respectively.

4. NMR and UV studies of anion recognition

Representative procedures of the titration experiments ($AdOPO_3Na_2$ (**G2**Na_2) to **1**$(OTf)_7$)

NMR titration and UV titration experiments to determine the binding constants were performed three times.

^{1}H NMR titration:

A host solution of **1**$(OTf)_7$ (2.0 mM) was prepared by adding **1**$(OTf)_7$ (3.13 mg, 1.01 μmol), D_2O (50 μL) and H_2O (450 μL) to an NMR tube. A guest solution of **G2**Na_2 (41.3 mM) was prepared by adding **G2**Na_2 (2.28 mg, 8.26 μmol), D_2O (20 μL) and H_2O (180 μL) to a microtube. 12.2 μL (0.504 μmol, 0.50 equiv.) each of the guest solution was titrated into the sample solution. ^{1}H NMR measurements (600 MHz, 298 K) were carried out during the titration.

UV-vis titration:

An aqueous solution of MES (406 μM) was prepared by adding MES·H_2O (8.66 mg, 40.6 μmol) and H_2O to a 100 mL volumetric flask. An aqueous solution of NaOH (23.4 mM) was prepared by adding NaOH (93.78 mg, 2.34 mmol) and H_2O to a 100 mL volumetric flask. Then, NaOH aq (0.28 mL) was added dropwise to the MES aq (100 mL) to give a MES buffer solution (0.38 mM, pH = 7.0).

A host solution of **1**$(OTf)_7$ (12 μM) was prepared by adding **1**$(OTf)_7$ (0.75 mg, 0.24 μmol) and MES buffer solution to a 20 mL volumetric flask. A solution of **G2**Na_2 (1.85 mM) was prepared by adding **G2**Na_2 (1.02 mg, 3.69 μmol) and the host solution of **1**$(OTf)_7$ (12 μM) to a 2 mL volumetric flask. A guest solution of **G2**Na_2 (249 μM) for the titration was prepared by adding 135 μL of the stock solution of **G2**Na_2 (1.85 mM) and the host solution of **1**$(OTf)_7$ (12 μM) to a 1 mL volumetric flask.

3.00 mL of the host solution was added to a 1.0 cm quartz cell, and the guest solution was titrated into the sample solution. UV-vis measurements (298 K) were carried out during the titration. The host concentration was kept constant at 12.0 μM.

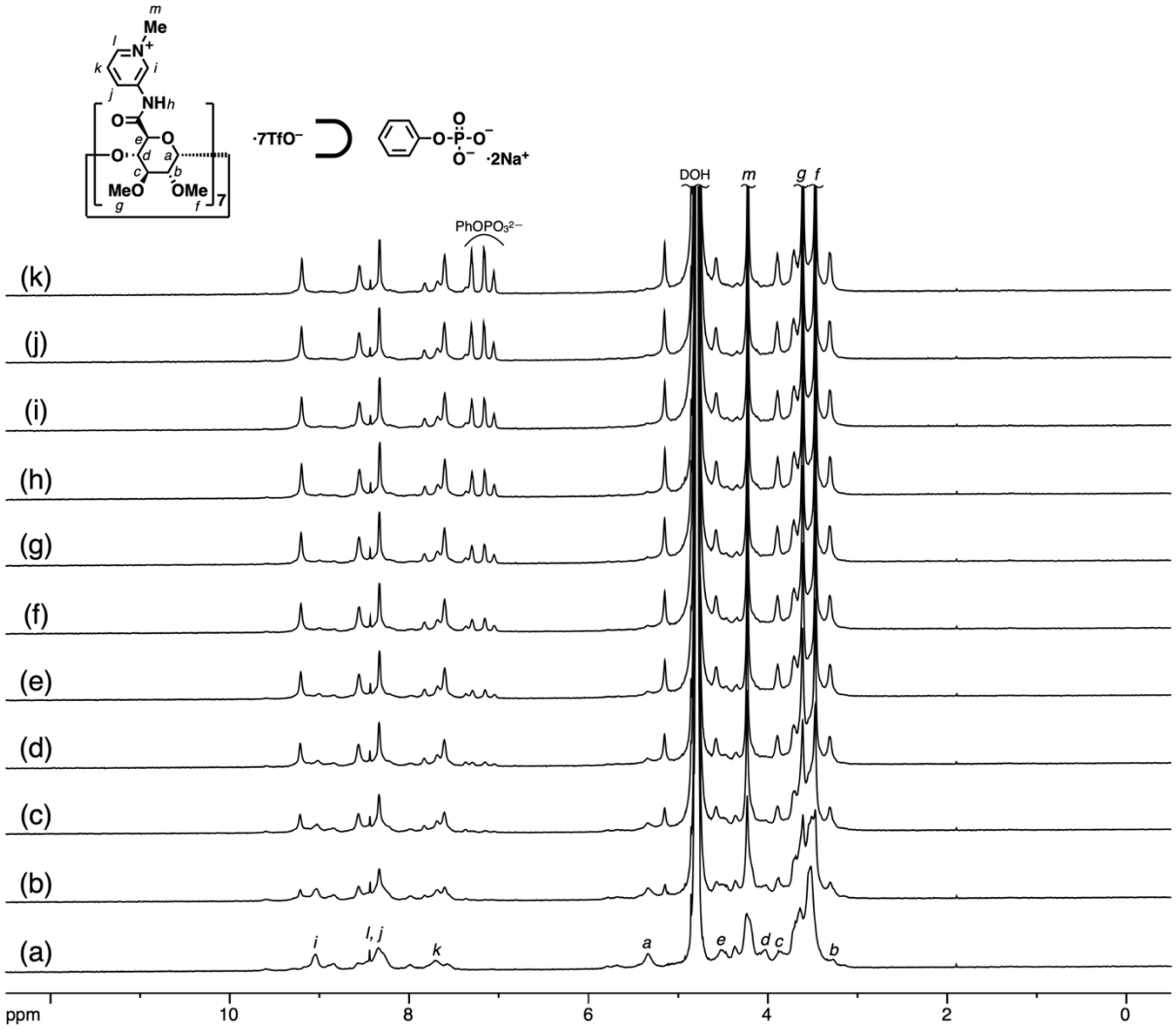

Figure S15. A titration experiment of $PhOPO_3Na_2$ (**G1**Na_2) against **1**$(OTf)_7$ (1.3 mM) (^{1}H NMR, D_2O, 600 MHz). (a) **1**$(OTf)_7$. (b–k) **1**$(OTf)_7$ + $PhOPO_3Na_2$. (b) $PhOPO_3Na_2$ 0.3 eq. (c) 0.5 eq. (d) 0.8 eq. (e) 1.0 eq. (f) 1.3 eq. (g) 1.5 eq. (h) 1.8 eq. (i) 2.0 eq. (j) 2.3 eq. (k) 2.5 eq.

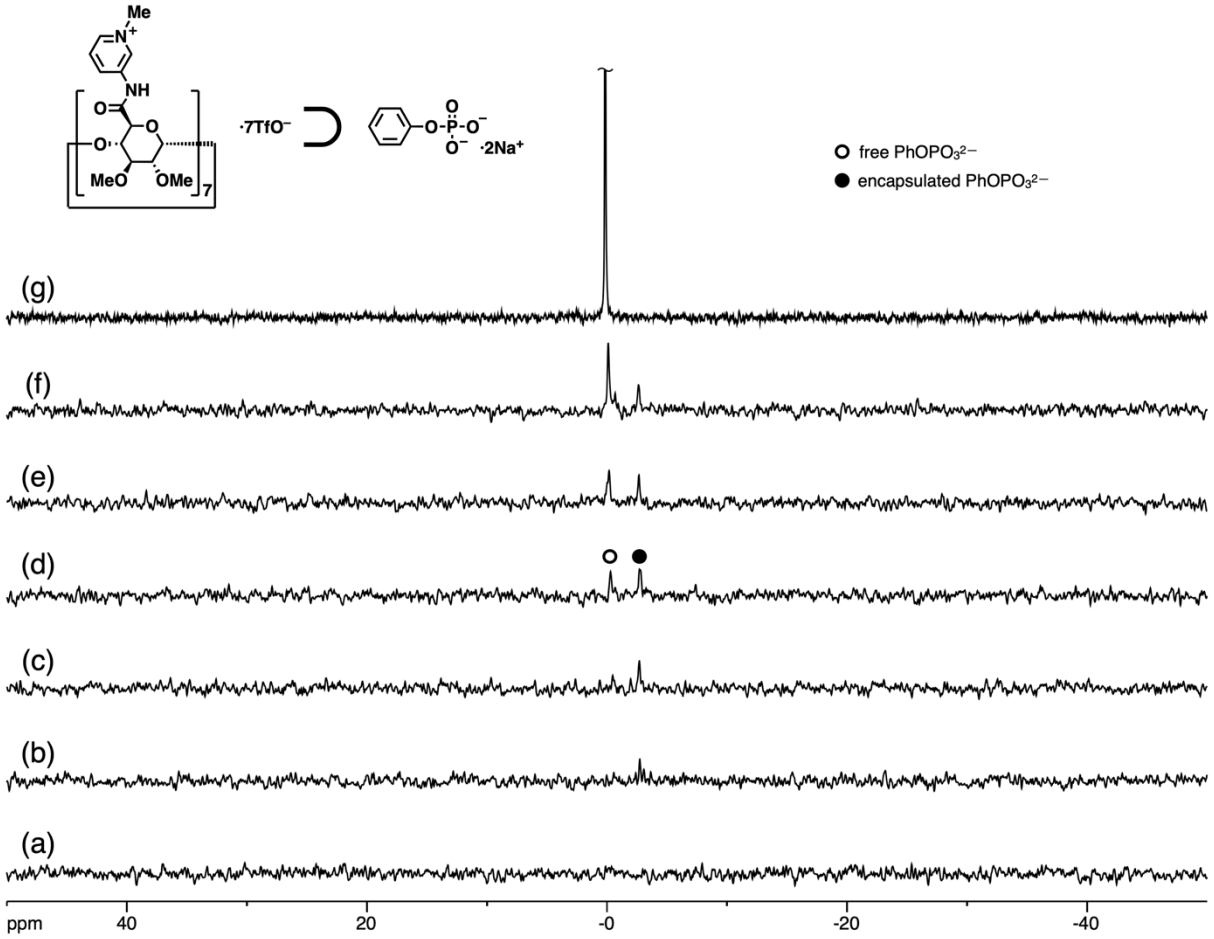

Figure S16. A titration experiment of $PhOPO_3Na_2$ (**G1**Na_2) against **1**$(OTf)_7$ (2.0 mM) (^{31}P NMR, D_2O, 162 MHz). (a) **1**$(OTf)_7$. (b−f) **1**$(OTf)_7$ + $PhOPO_3Na_2$. (b) $PhOPO_3Na_2$ 0.5 eq. (c) 1.0 eq. (d) 1.5 eq. (e) 2.0 eq. (f) 3.0 eq. (g) $PhOPO_3Na_2$ (**G1**Na_2).

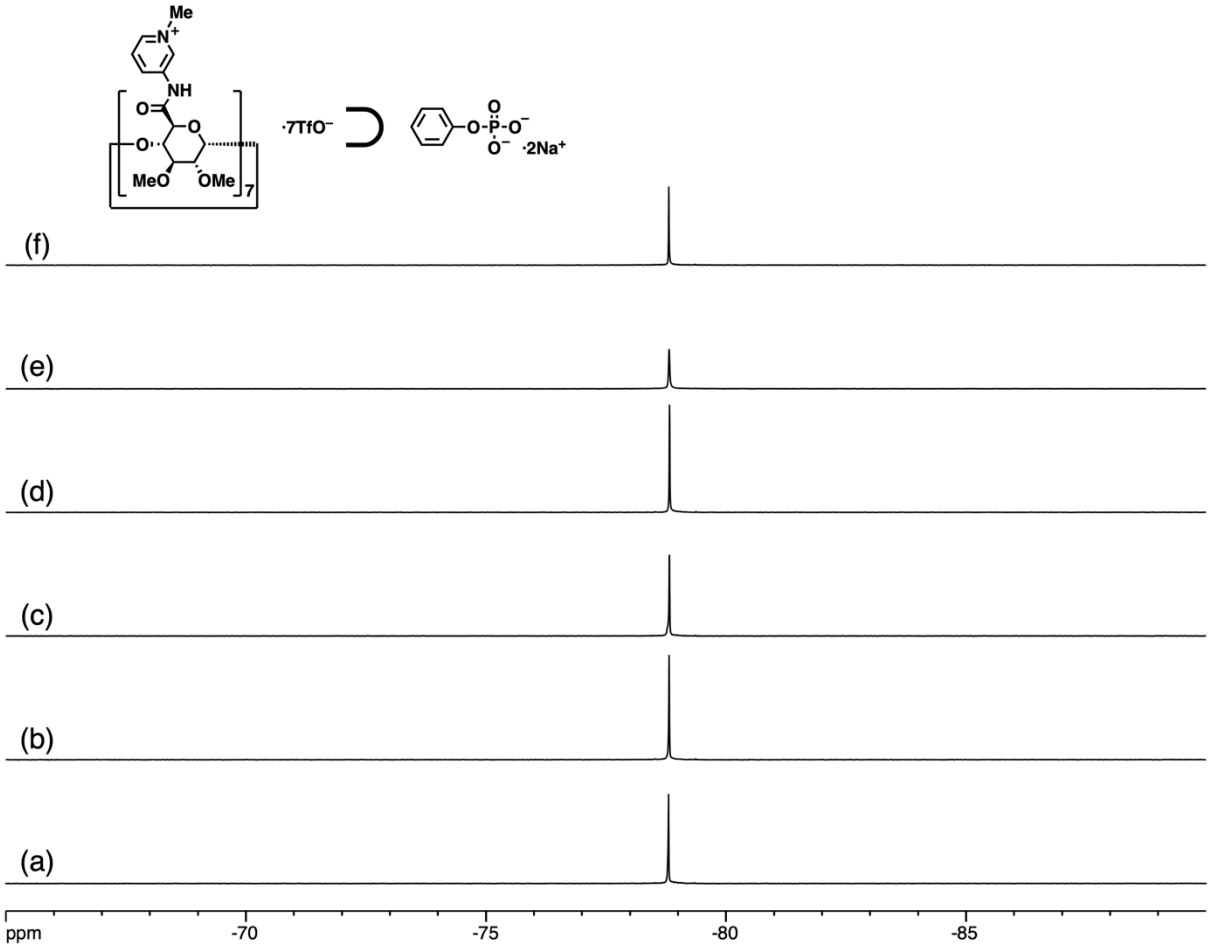

Figure S17. A titration experiment of $PhOPO_3Na_2$ (**G1**Na_2) against **1**$(OTf)_7$ (2.0 mM) (^{19}F NMR, D_2O, 376 MHz). (a) **1**$(OTf)_7$. (b−f) **1**$(OTf)_7$ + $PhOPO_3Na_2$. (b) $PhOPO_3Na_2$ 0.5 eq. (c) 1.0 eq. (d) 1.5 eq. (e) 2.0 eq. (f) 3.0 eq.

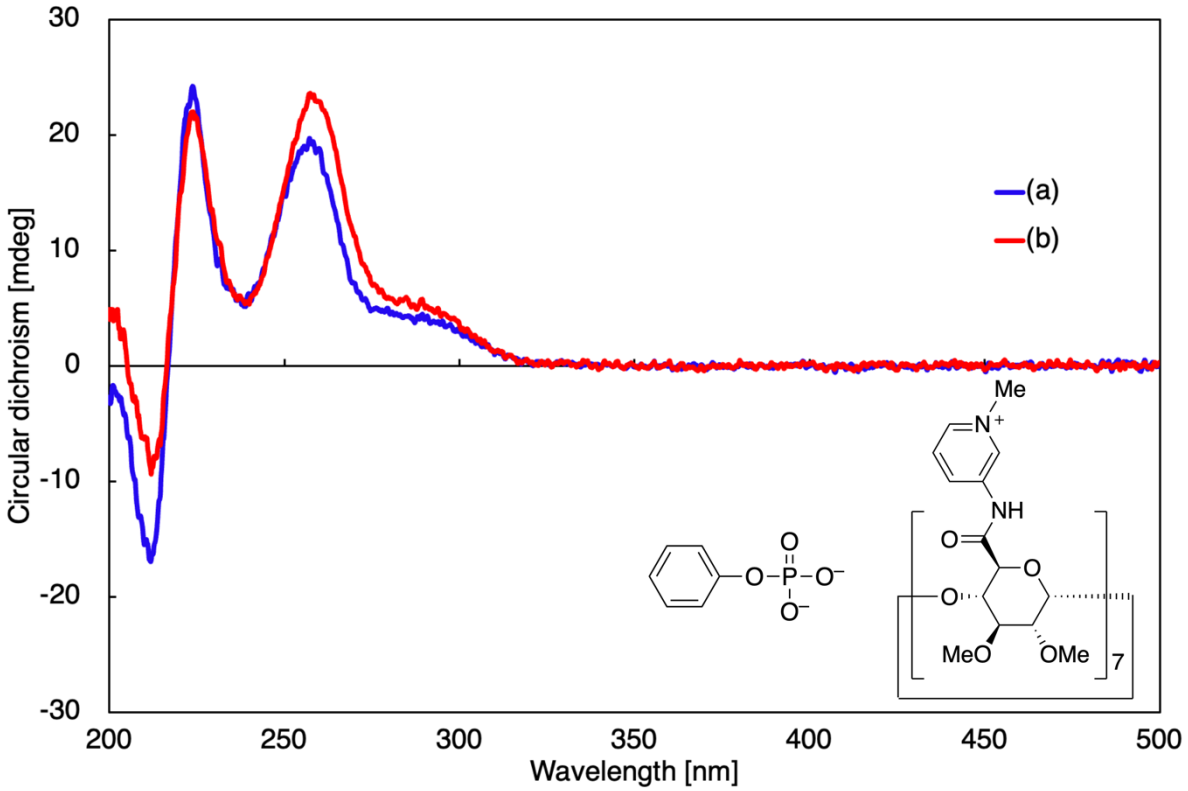

Figure S18. Circular dichroism spectral change of **1**$(OTf)_7$ upon recognition of $PhOPO_3Na_2$ (**G1**Na_2) ([**1**$(OTf)_7$] = 11 μM, H_2O, r.t., l = 1 cm). (a) **1**$(OTf)_7$. (b) **1**$(OTf)_7$ + **G1**Na_2 (2.1 equiv.).

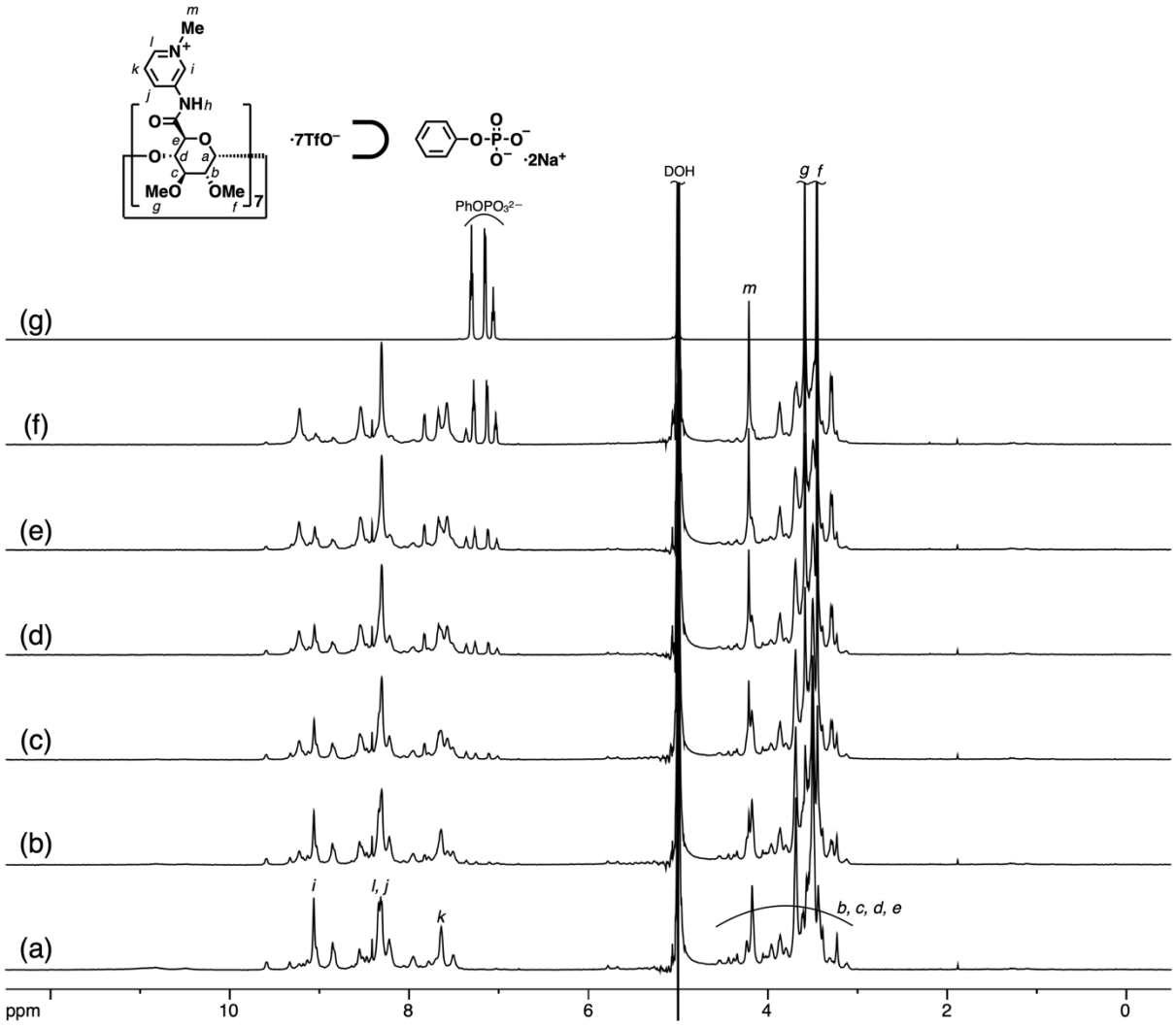

Figure S19. A titration experiment of $PhOPO_3Na_2$ (**G1**Na_2) against **1**$(OTf)_7$ (2.0 mM) in H_2O/D_2O = 9/1 (^{1}H NMR (WATERGATE), 278 K, 600 MHz). (a) **1**$(OTf)_7$. (b–f) **1**$(OTf)_7$ + $PhOPO_3Na_2$. (b) $PhOPO_3Na_2$ 0.3 eq. (c) 0.5 eq. (d) 0.8 eq. (e) 1.0 eq. (f) 2.0 eq. (g) $PhOPO_3Na_2$ (**G1**Na_2).

Synthesis of 1-adamantyl dibenzyl phosphate (**5**)

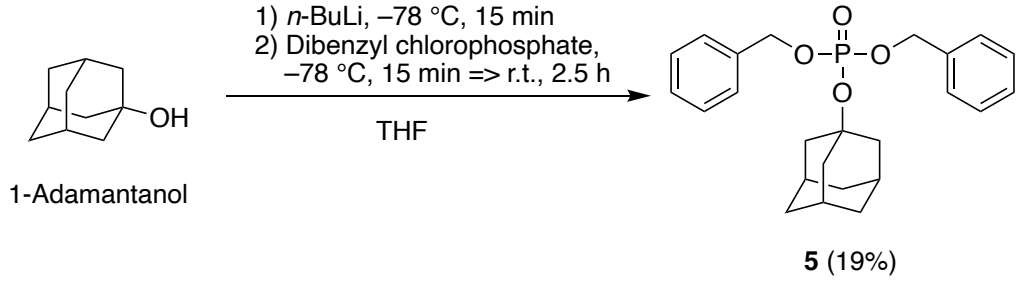

Scheme S3. Synthesis of 1-adamantyl dibenzyl phosphate (**5**)

1-Adamantanol (767.6 mg, 5.04 mmol, 1.0 equiv) was added to a 100 mL 2-necked pear-shaped flask, and the atmosphere was replaced with argon. Dry THF (20 mL) was added to the flask, and the solution was stirred at –78 °C. Then, 1.39 M hexane solution of *n*-BuLi (3.99 mL, 5.55 mmol, 1.1 equiv) was added to the flask, and the mixture was stirred at –78 °C for 15 min. Then, THF solution (10 mL) of dibenzyl chlorophosphate[S7] (1.496 g, 5.04 mmol, 1.0 equiv) was added via cannulation, and the mixture was stirred at –78 °C for 15 min and at room temperature for 2.5 h. H_2O (20 mL) was added to the flask and the mixture was transferred to a separating funnel and extracted with Et_2O (20 mL × 3). The combined organic layer was washed with H_2O (60 mL) and the organic layer was dried over Na_2SO_4 then concentrated in vacuo. The residue was purified by flash column chromatography (eluent: $CHCl_3$/AcOEt = 100/0−90/10). The obtained fractions were concentrated in vacuo, then the residue was further purified by flash column chromatography (eluent: $CHCl_3$/AcOEt = 100/0−92/8). The obtained fractions were concentrated in vacuo to give 1-adamantyl dibenzyl phosphate (**5**)[S8] (404.5 mg, 0.981 mmol, 19%).

Pale yellow oil;

^{1}H NMR ($CDCl_3$, 600 MHz): δ 7.34 (m, 10H), 5.00 (br, 4H), 2.17 (br, 3H), 2.06 (br, 6H), 1.61 (br, 6H);

^{13}C NMR ($CDCl_3$, 101 MHz): δ 136.3, 128.5, 128.2, 127.8, 82.7, 68.7, 43.4, 35.7, 31.1;

^{31}P NMR ($CDCl_3$, 243 MHz): δ –5.6;

HRMS (ESI): *m/z* $[M+Na]^+$ calcd. for $C_{24}H_{29}O_4PNa$ 435.1701, found 435.1685;

Synthesis of 1-adamantyl phosphate (H_2**G2**)

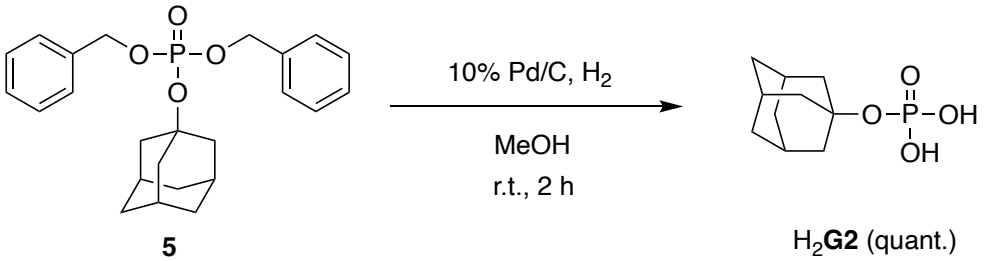

Scheme S4. Synthesis of 1-adamantyl phosphate (H_2**G2**)

1-Adamantyl dibenzyl phosphate (**5**) (100.2 mg, 0.243 mmol, 1.0 equiv) was added to a 30 mL eggplant flask, and MeOH (4 mL) and 10% Pd/C (30.4 mg) were added to the flask. The atmosphere was replaced with H_2, and the mixture was stirred at room temperature for 2 h. Then, the mixture was filtrated through celite, and the filtrate was concentrated in vacuo to give 1-adamantyl phosphate (H_2**G2**) (51.2 mg, quant.).
White solid;
^{1}H NMR (CD_3OD, 600 MHz): δ 2.16 (br, 3H), 2.08 (br, 6H), 1.68 (br, 6H);
^{13}C NMR (CD_3OD, 151 MHz): δ 80.9, 44.5, 37.0, 32.5;
^{31}P NMR (CD_3OD, 243 MHz): δ –3.9.

Synthesis of disodium 1-adamantyl phosphate (**G2**Na_2)

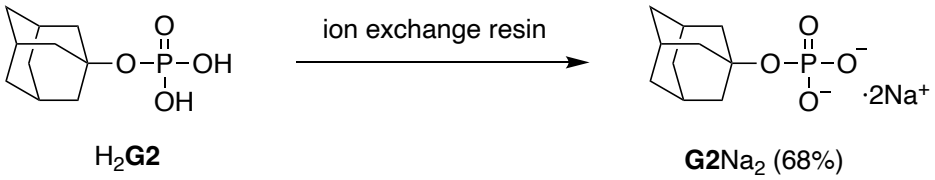

Scheme S5. Synthesis of disodium 1-adamantyl phosphate (**G2**Na_2)

A solution of 1-adamantyl phosphate (H_2**G2**) (41.2 mg, 0.237 mmol) in H_2O:MeOH = 1:1 was passed through the ion exchange column by elution with H_2O:MeOH = 1:1 (before the column, the cation exchange resin of H^+ form was passed 7–8 CV (column volume) of H_2O, 6–7 CV of 1 M NaCl aq, then the resin was washed with 9–10 CV of H_2O, and substituted by 4–5 CV of H_2O:MeOH = 1:1). The obtained solution was concentrated in vacuo to give disodium 1-adamantyl phosphate (**G2**Na_2) (44.6 mg, 0.161 mmol, 68%).
White solid;
^{1}H NMR (CD_3OD, 600 MHz): δ 2.13 (br, 3H), 2.08 (br, 6H), 1.67 (br, 6H);
^{13}C NMR (CD_3OD, 151 MHz): δ 78.0, 44.7, 37.2, 32.5;
^{31}P NMR (CD_3OD, 243 MHz): δ –3.4;
HRMS (ESI): *m/z* $[M+H]^+$ calcd. for $C_{10}H_{16}O_4PNa_2$ 277.0582, found 277.0564.

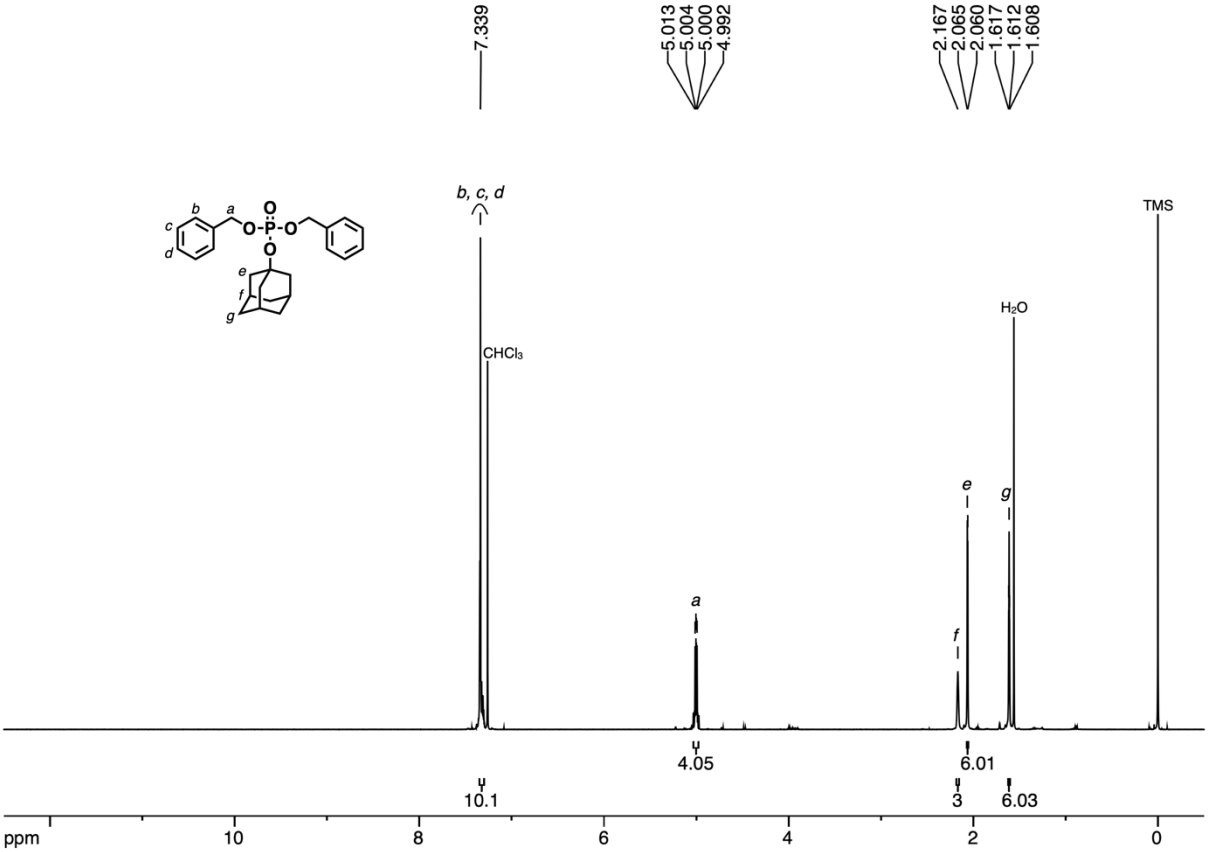

Figure S20. ^{1}H NMR spectrum of 1-adamantyl dibenzyl phosphate ($CDCl_3$, 600 MHz)

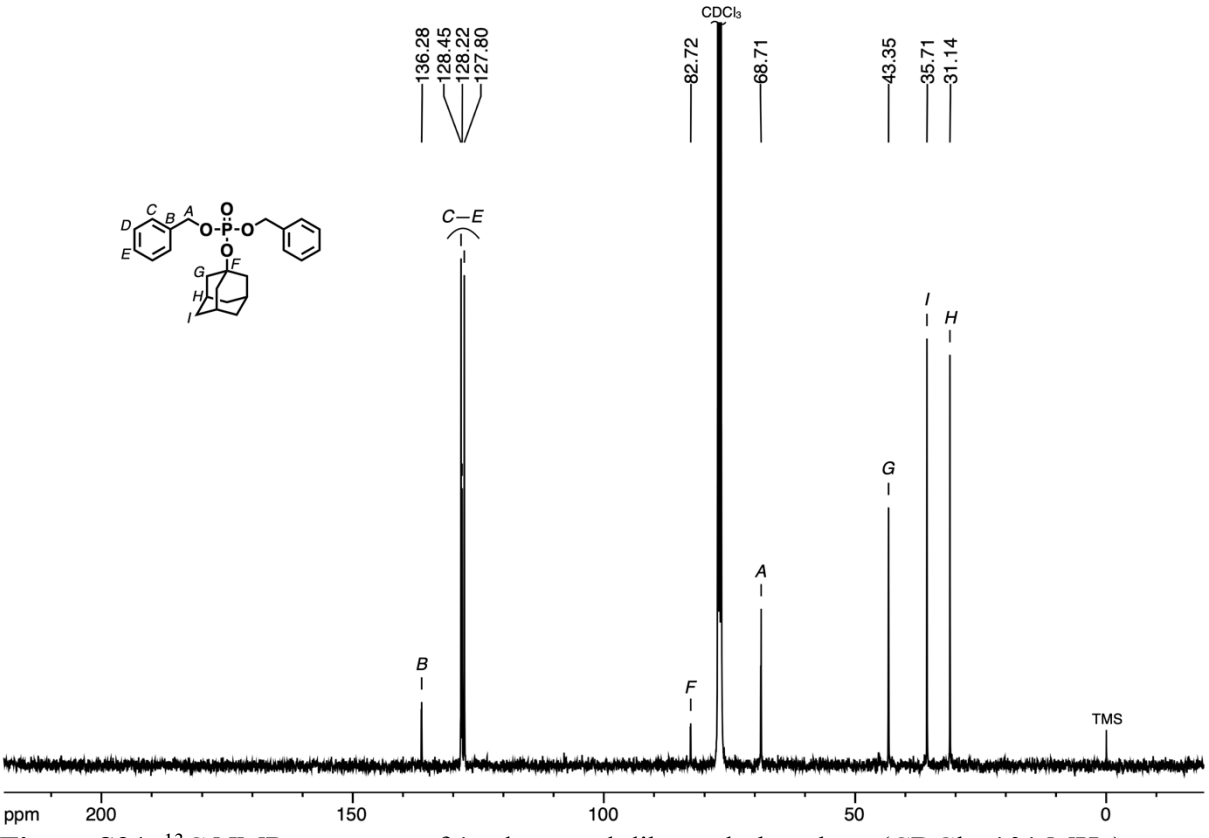

Figure S21. ^{13}C NMR spectrum of 1-adamantyl dibenzyl phosphate ($CDCl_3$, 101 MHz)

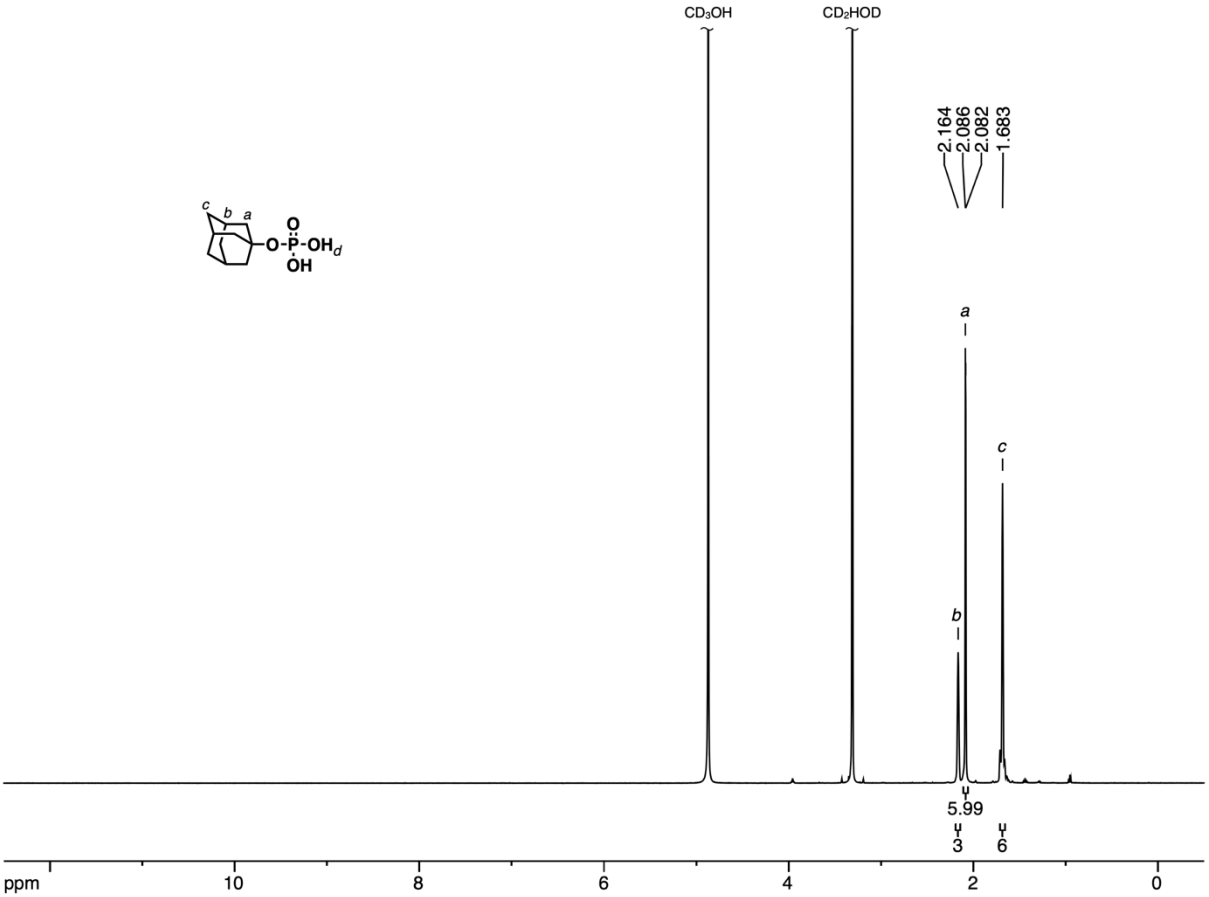

Figure S22. ^{1}H NMR spectrum of 1-adamantyl phosphate (CD_3OD, 600 MHz).

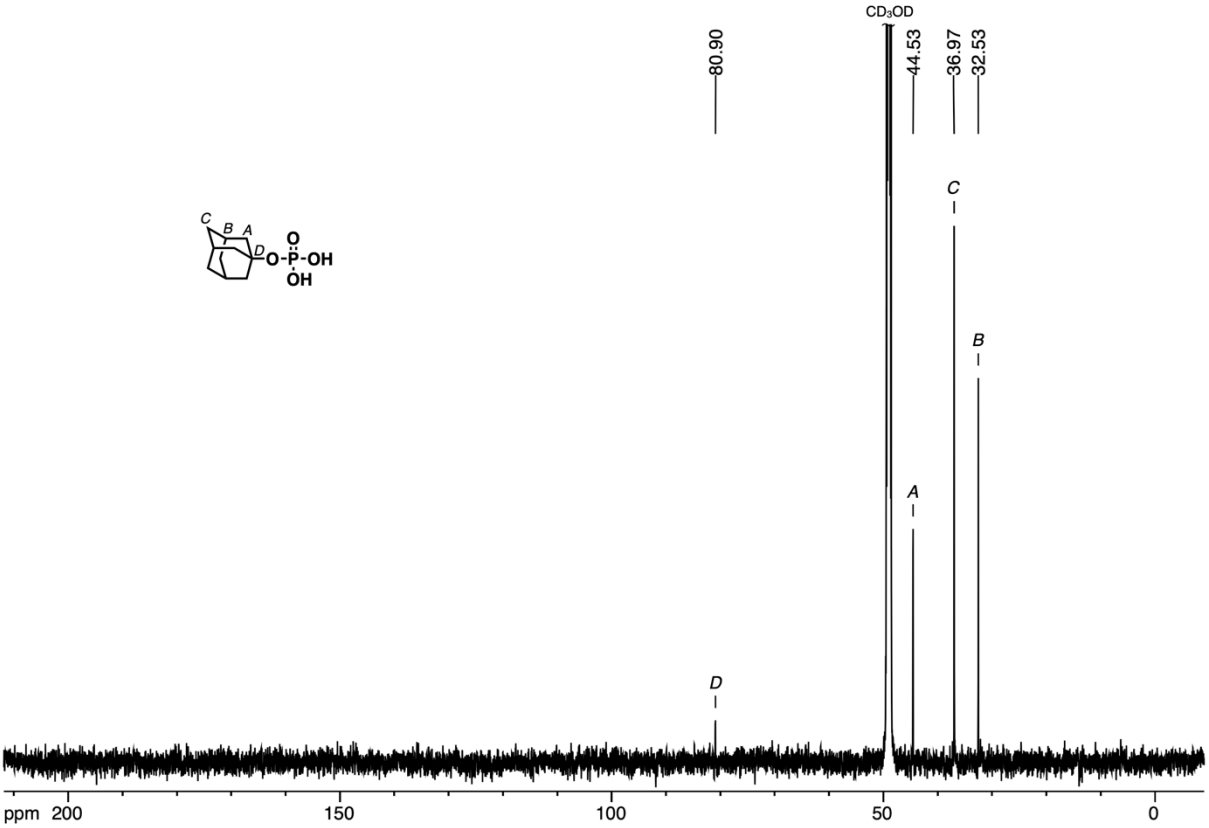

Figure S23. ^{13}C NMR spectrum of 1-adamantyl phosphate (CD_3OD, 151 MHz)

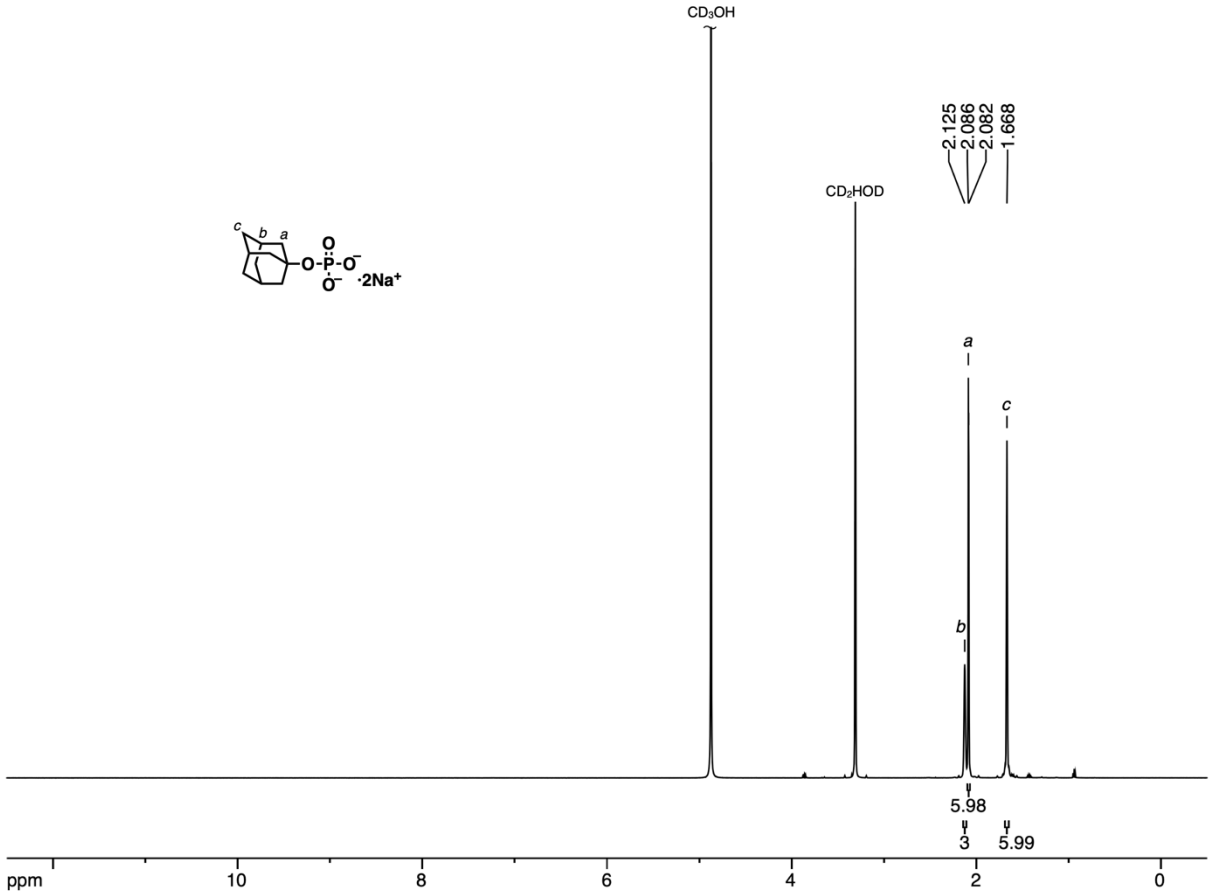

Figure S24. ^{1}H NMR spectrum of disodium 1-adamantyl phosphate (**G2**Na_2) (CD_3OD, 600 MHz).

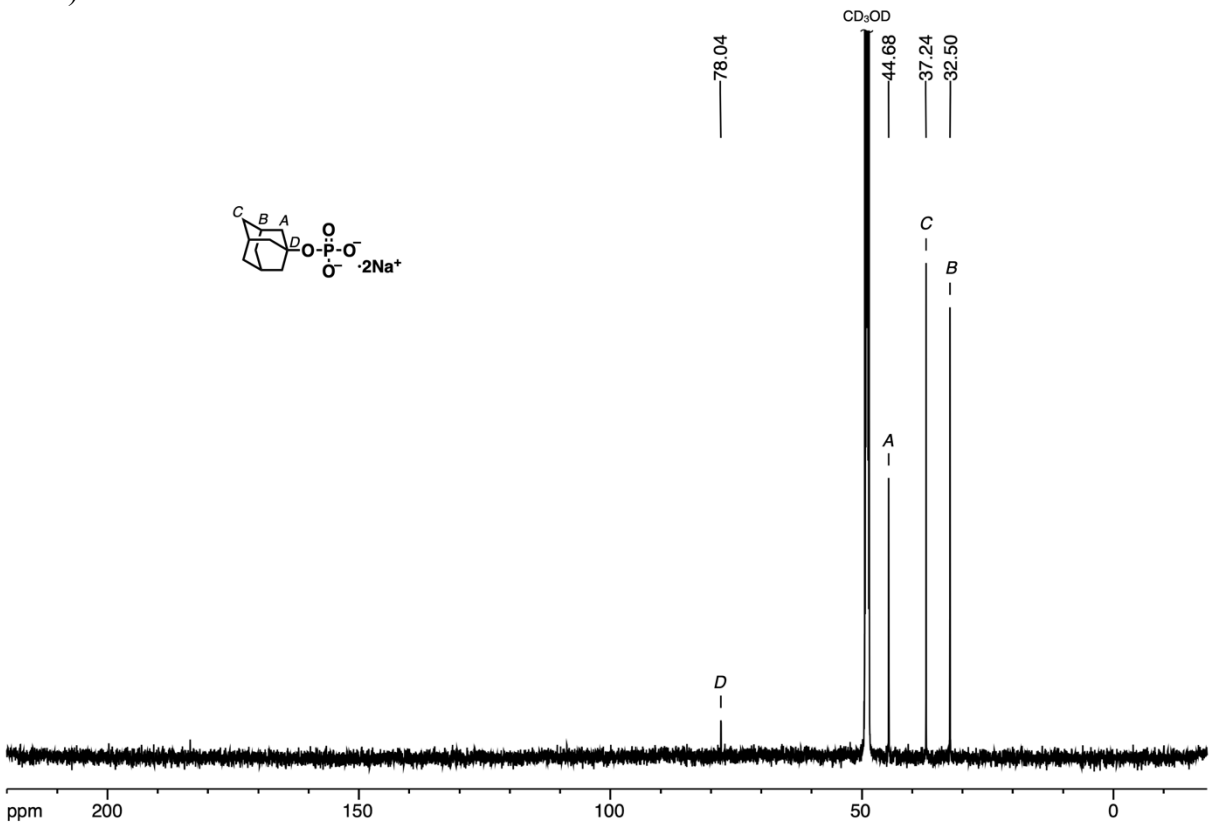

Figure S25. ^{13}C NMR spectrum of disodium 1-adamantyl phosphate (**G2**Na_2) (CD_3OD, 151 MHz).

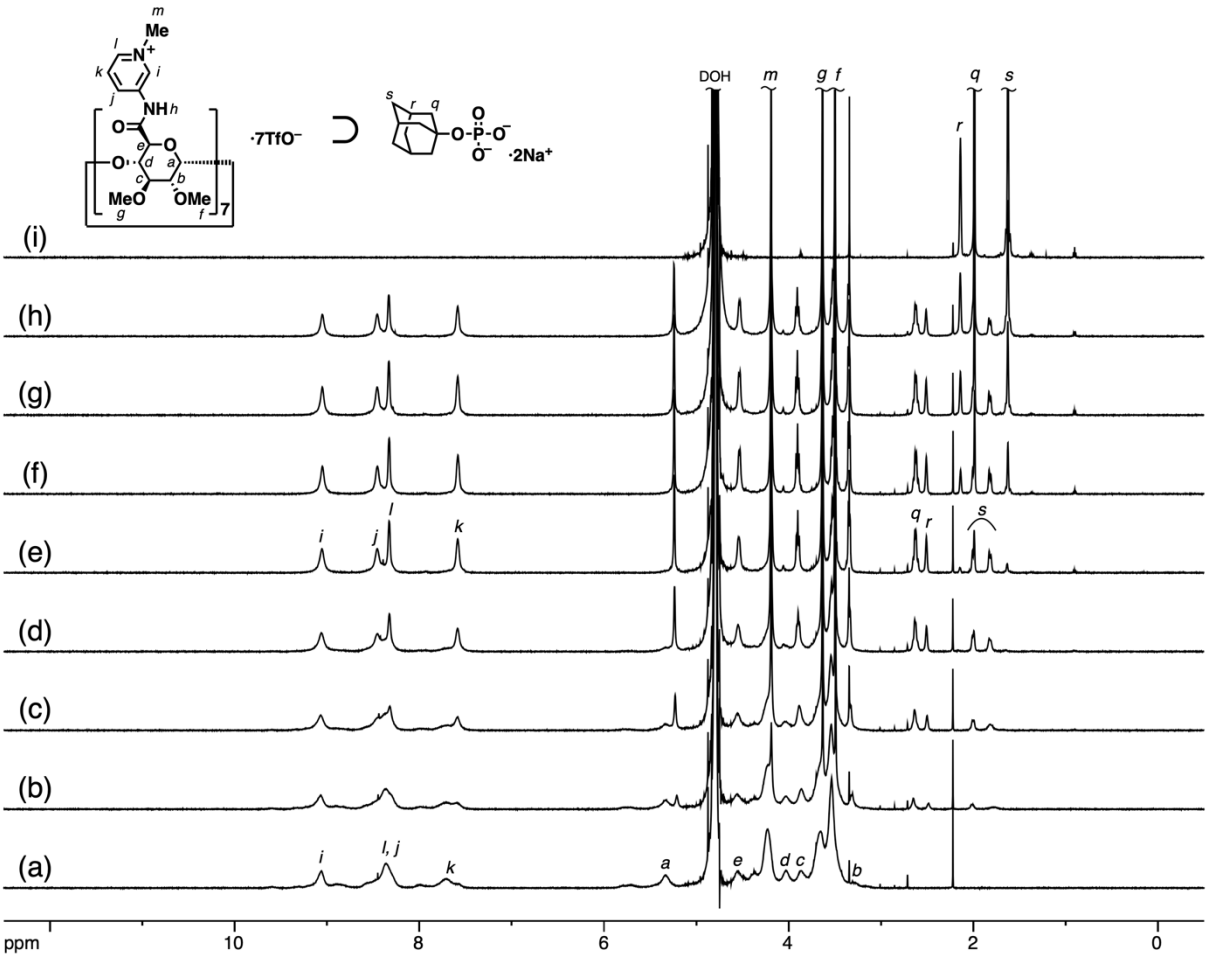

Figure S26. A titration experiment of $AdOPO_3Na_2$ (**G2**Na_2) against **1**$(OTf)_7$ (2.0 mM) (^{1}H NMR, D_2O, 600 MHz). (a) **1**$(OTf)_7$. (b−h) **1**$(OTf)_7$ + $AdOPO_3Na_2$. (b) $AdOPO_3Na_2$ 0.3 eq. (c) 0.5 eq. (d) 0.8 eq. (e) 1.0 eq. (f) 1.5 eq. (g) 2.0 eq. (h) 3.0 eq. (i) $AdOPO_3Na_2$ (**G2**Na_2).

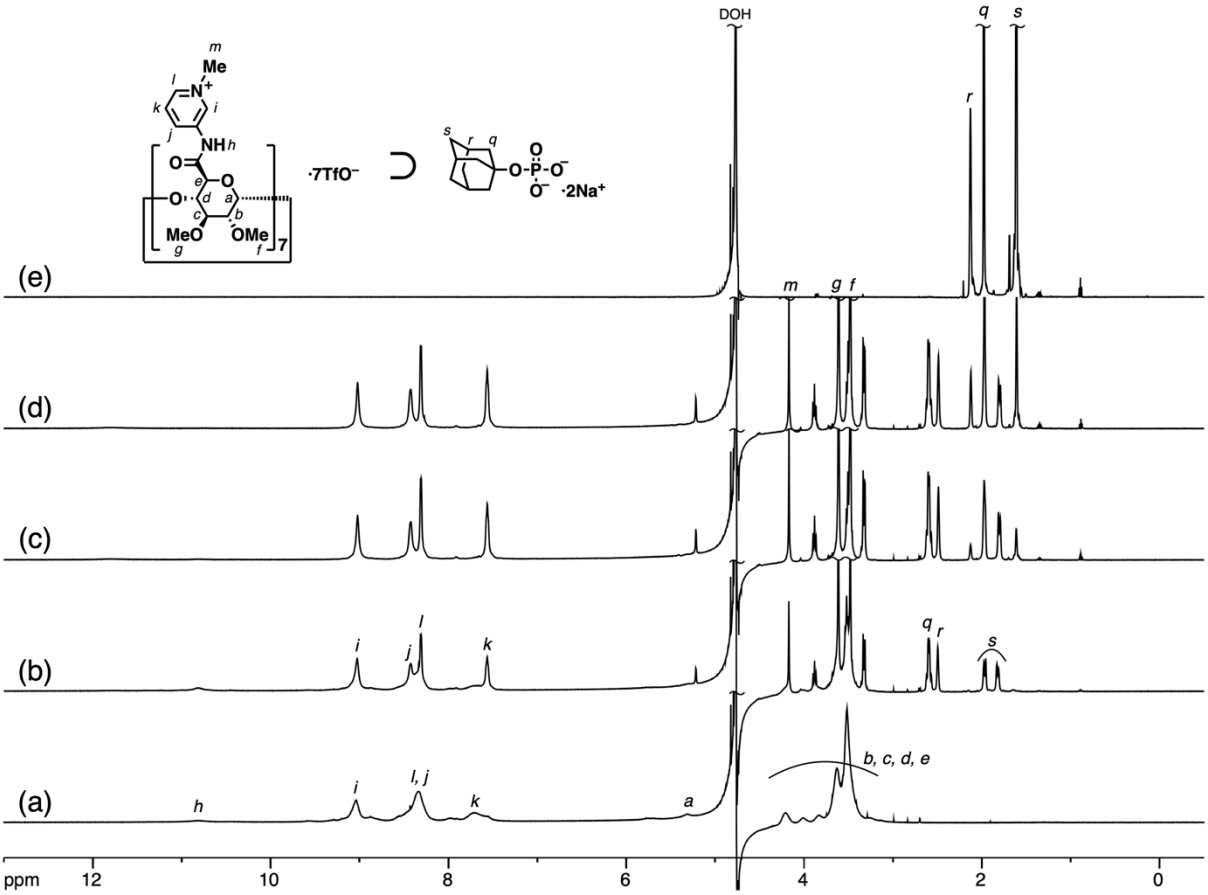

Figure S27. A titration experiment of $AdOPO_3Na_2$ (**G2**Na_2) against **1**$(OTf)_7$ (2.0 mM) (^{1}H NMR, H_2O/D_2O = 9/1, 600 MHz). (a) **1**$(OTf)_7$. (b−d) **1**$(OTf)_7$ + $AdOPO_3Na_2$. (b) $AdOPO_3Na_2$ 0.5 eq. (c) 1.0 eq. (d) 1.5 eq. (e) $AdOPO_3Na_2$ (**G2**Na_2).

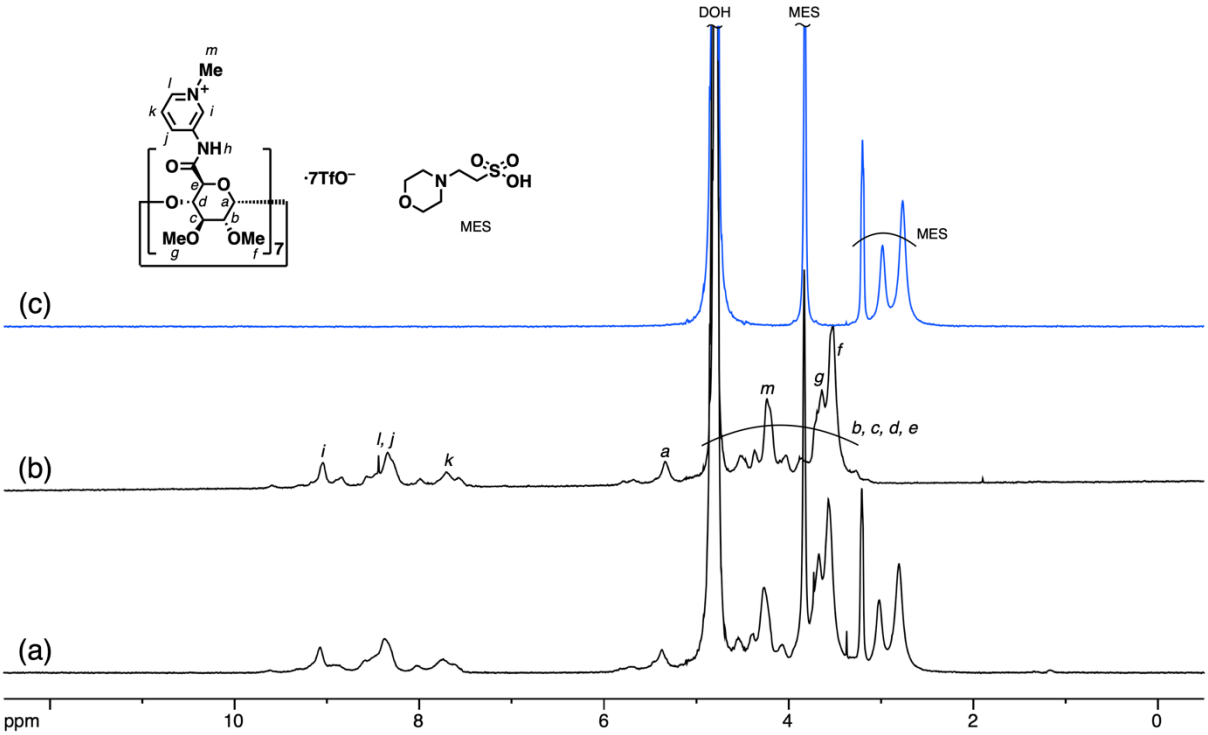

Figure S28. ^{1}H NMR spectra of **1**(OTf)$_7$ and MES (2-morpholinoethanesulfonic acid) (^{1}H NMR, 600 MHz). (a) **1**(OTf)$_7$ in 7.3 mM MES buffer with D_2O (adjusted with NaOD, pD = 7.5). (b) **1**(OTf)$_7$ in D_2O. (c) 7.3 mM MES buffer with D_2O.

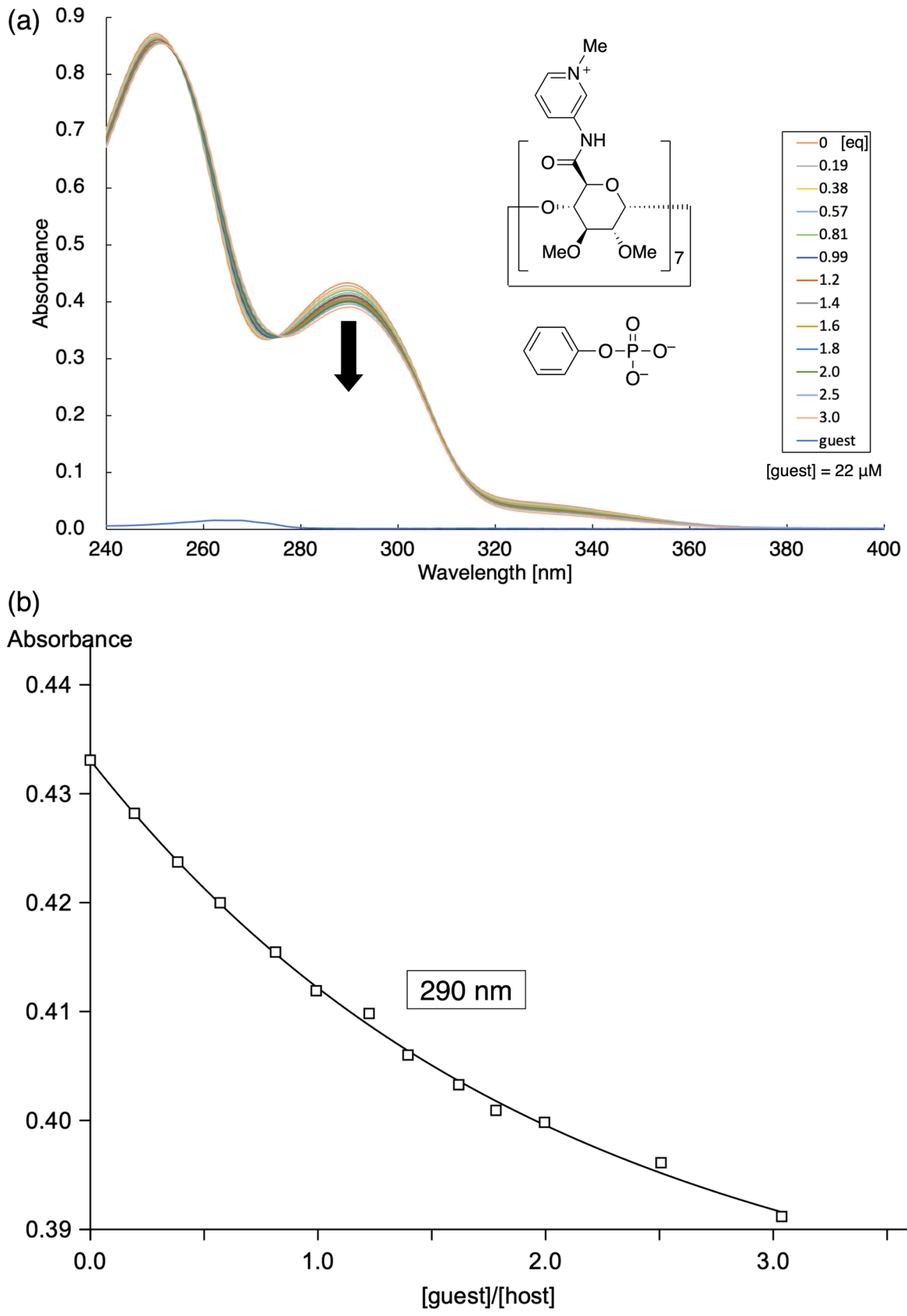

Figure S29. A titration experiment of $PhOPO_3Na_2$ (**G1**Na_2) against **1**$(OTf)_7$ (12 μM) (UV-vis, 0.38 mM MES buffer (pH = 7.0), *l* = 1 cm). (a) UV-vis absorbance spectra. (b) A least square fitting to determine the binding constant *K* between **G1**Na_2 and $\mathbf{1}^{7+}$ (data at λ_{abs} = 290 nm).

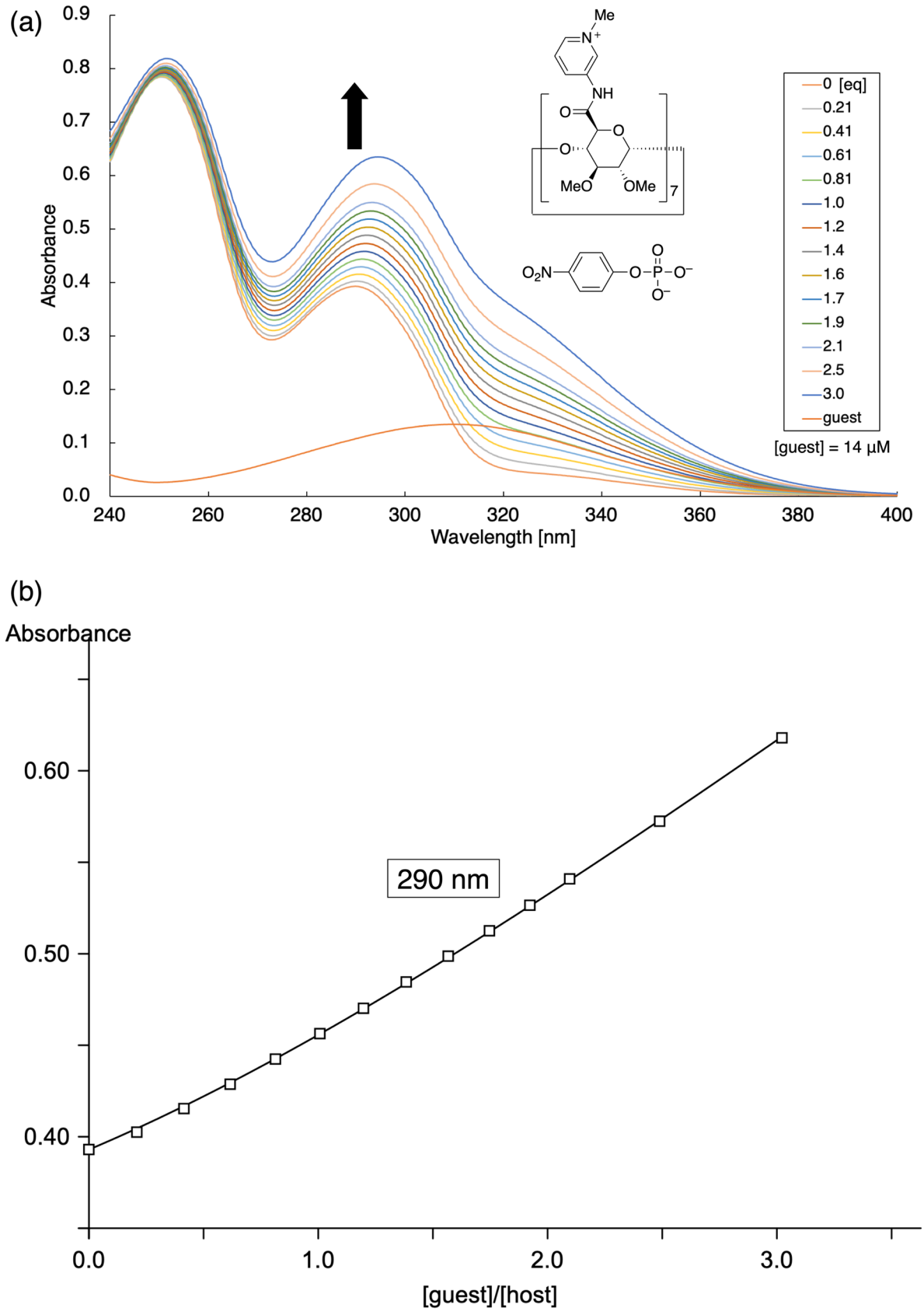

Figure S30. A titration experiment of **G3**Na_2 against **1**$(OTf)_7$ (12 µM) (UV-vis, 0.38 mM MES buffer (pH = 7.0), l = 1 cm). (a) UV-vis absorbance spectra. (b) A least square fitting to determine the binding constant K between **G3**Na_2 and $\mathbf{1}^{7+}$ (data at λ_{abs} = 290 nm).

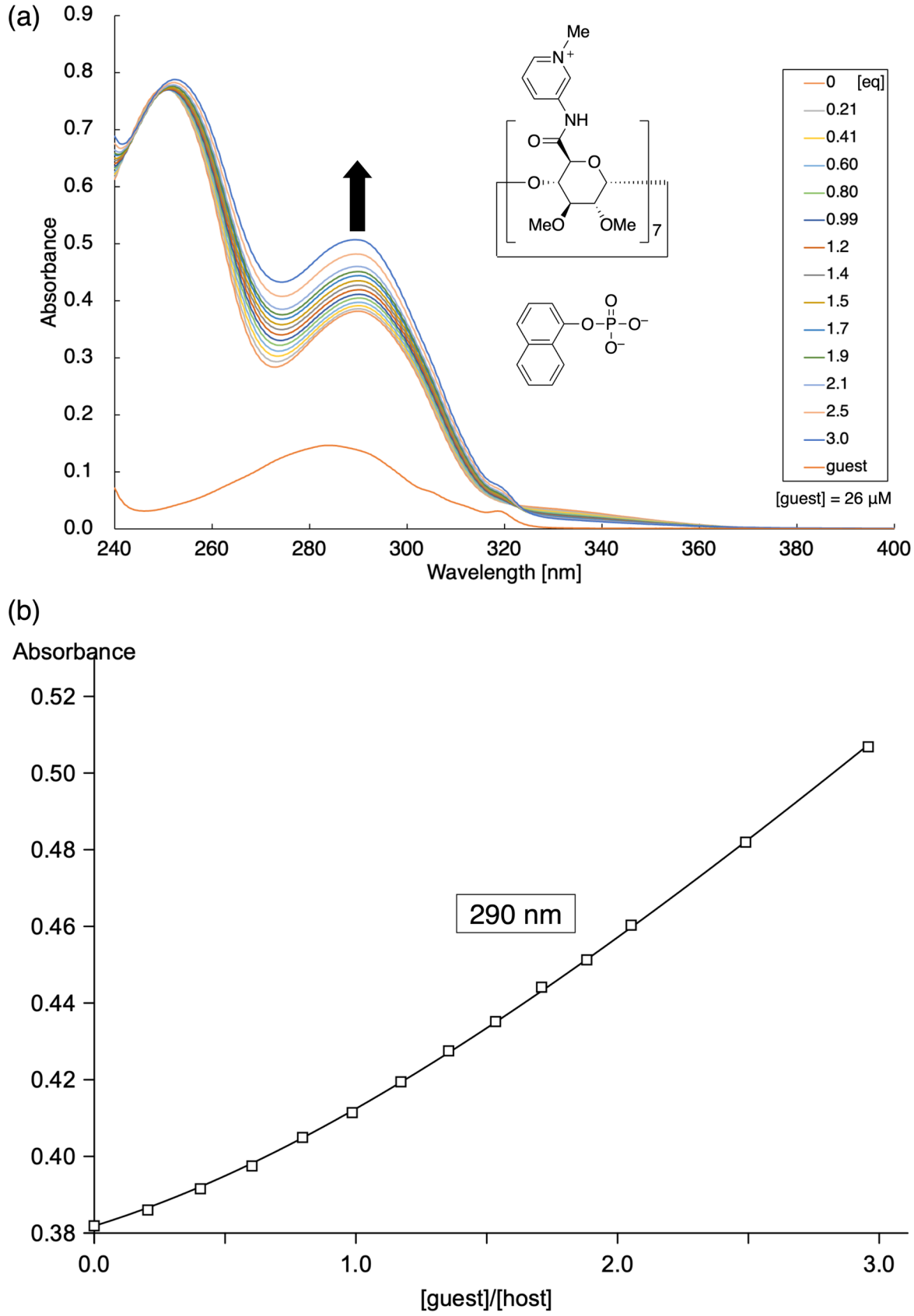

Figure S31. A titration experiment of **G4**HNa against **1**$(OTf)_7$ (12 μM) (UV-vis, 0.38 mM MES buffer (pH = 7.0), l = 1 cm). (a) UV-vis absorbance spectra. (b) A least square fitting to determine the binding constant K between **G4**HNa and $\mathbf{1}^{7+}$ (data at λ_{abs} = 290 nm).

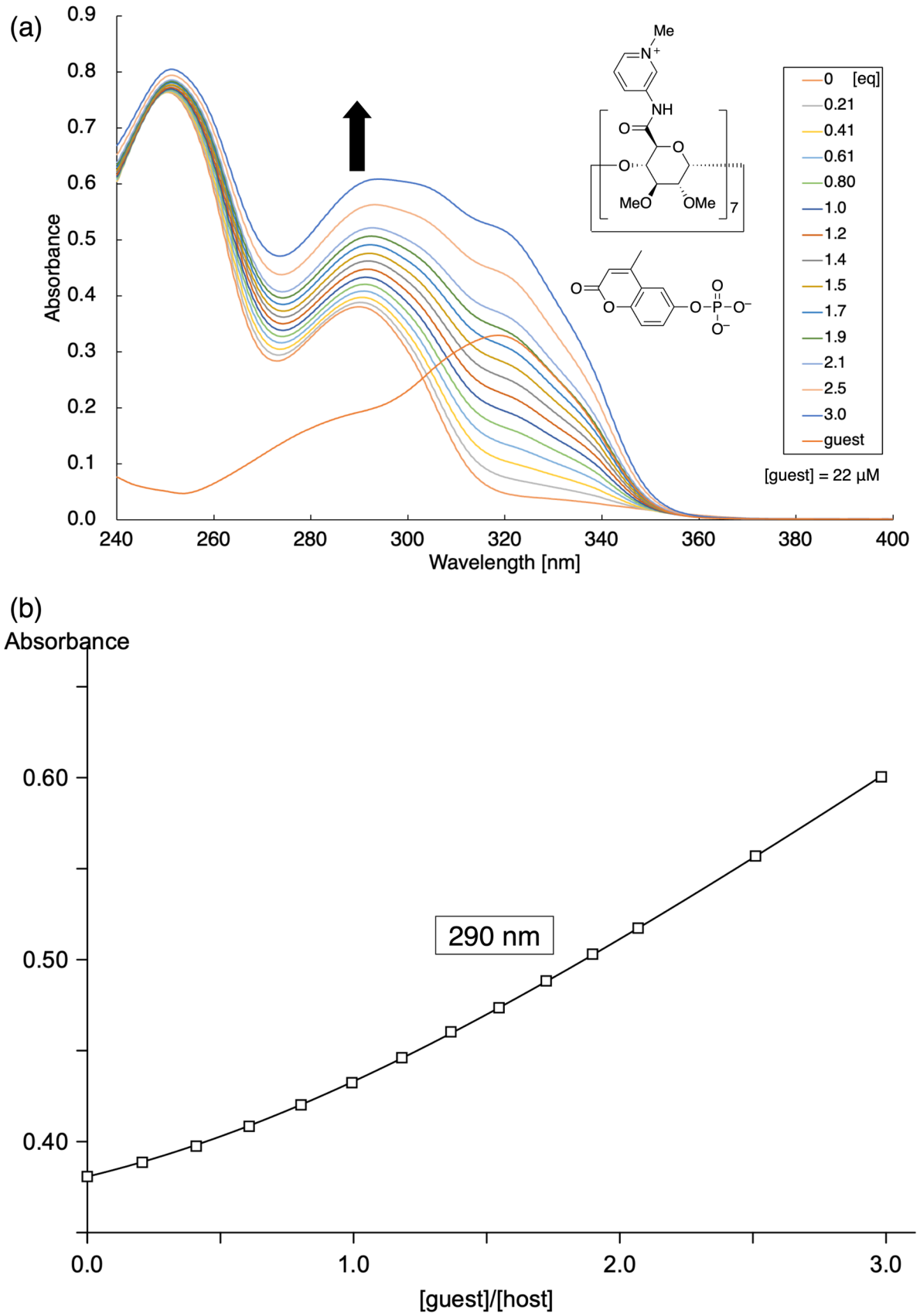

Figure S32. A titration experiment of H_2**G5** against **1**$(OTf)_7$ (12 μM) (UV-vis, 0.38 mM MES buffer (pH = 7.0), l = 1 cm). (a) UV-vis absorbance spectra. (b) A least square fitting to determine the binding constant K between H_2**G5** and $\mathbf{1}^{7+}$ (data at λ_{abs} = 290 nm).

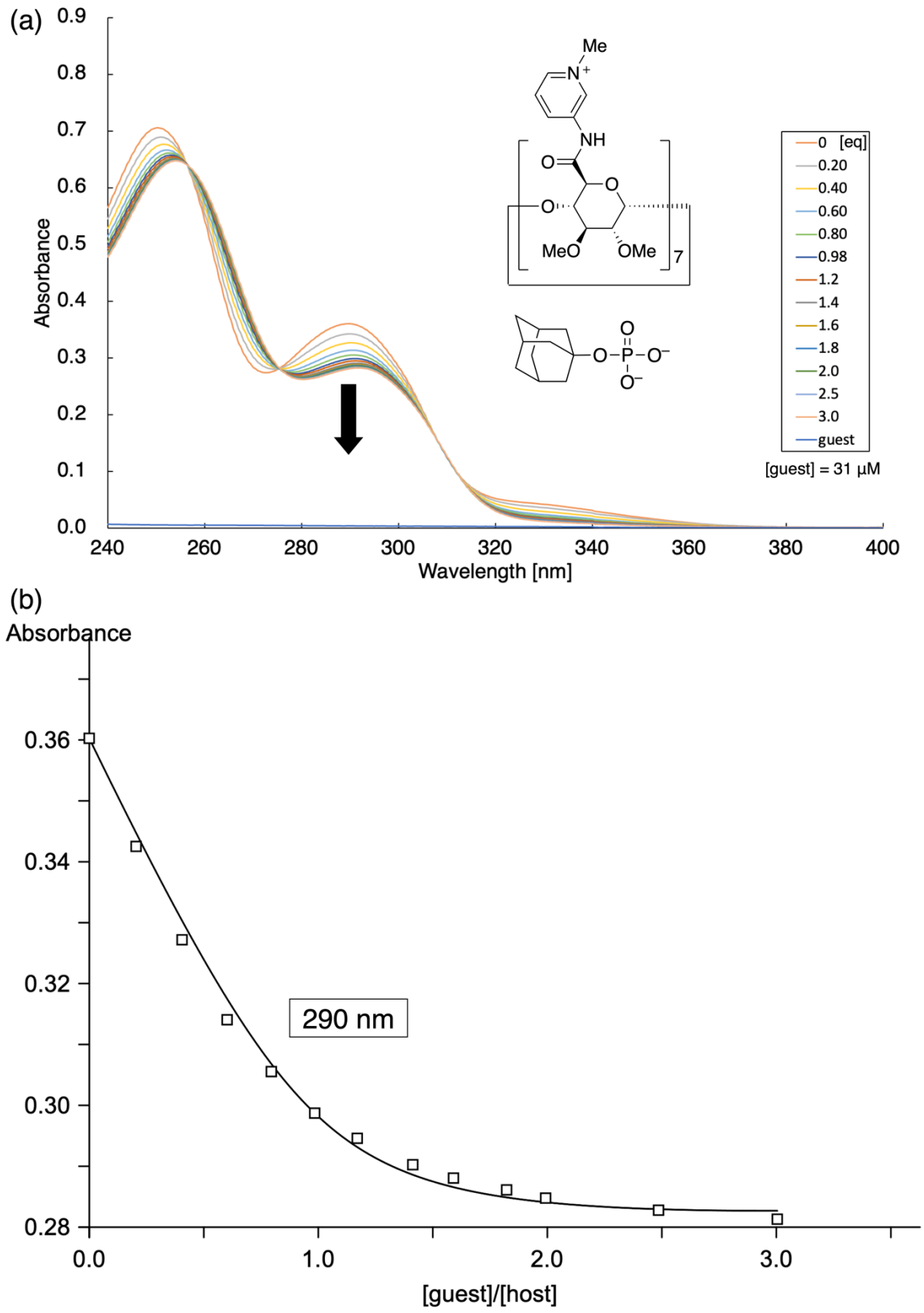

Figure S33. A titration experiment of $AdOPO_3Na_2$ (**G2**Na_2) against **1**$(OTf)_7$ (12 μM) (UV-vis, 0.38 mM MES buffer (pH = 7.0), l = 1 cm). (a) UV-vis absorbance spectra. (b) A least square fitting to determine the binding constant K between **G2**Na_2 and $\mathbf{1}^{7+}$ (data at λ_{abs} = 290 nm).

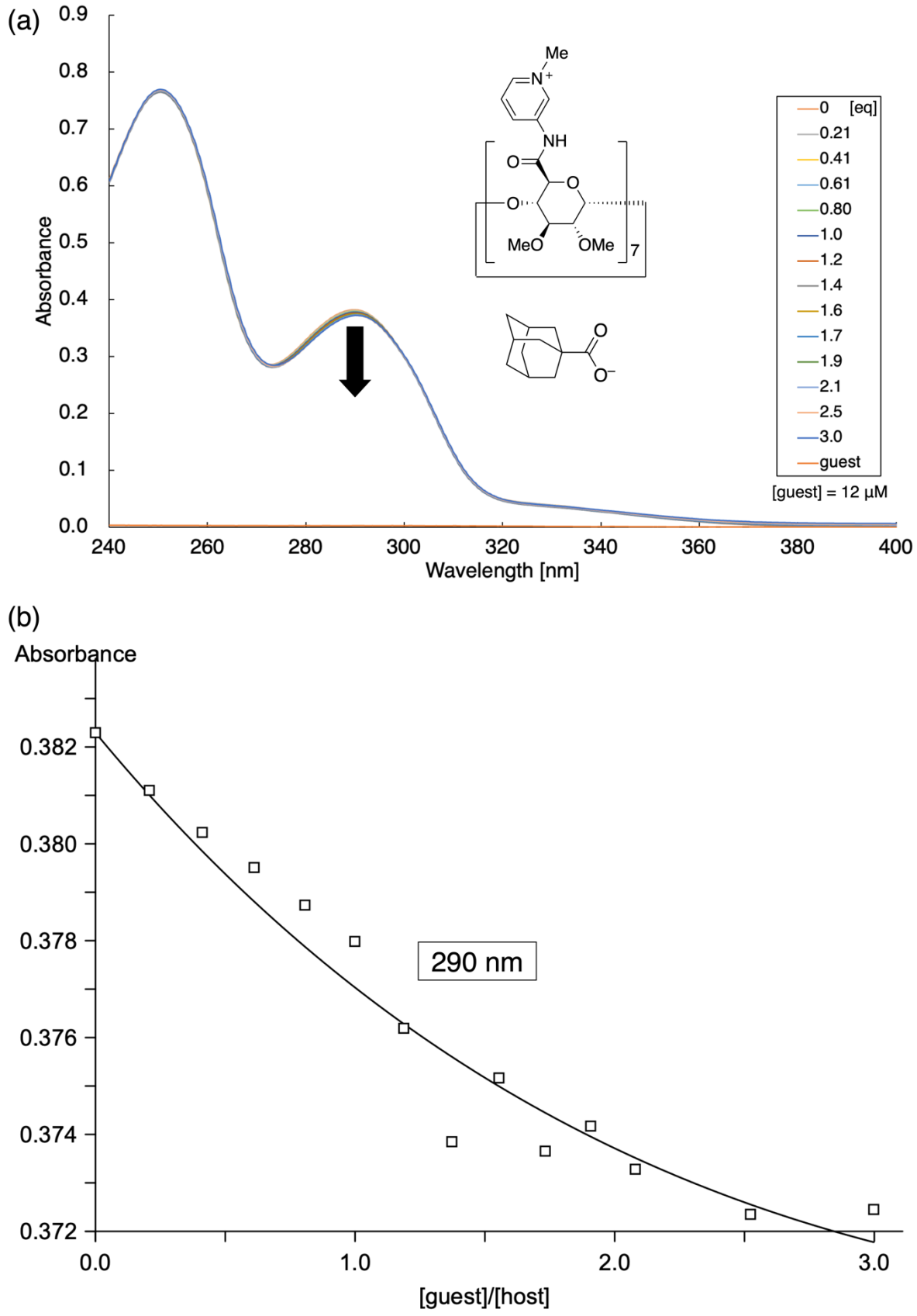

Figure S34. A titration experiment of H**G6** against **1**$(OTf)_7$ (12 μM) (UV-vis, 0.38 mM MES buffer (pH = 7.0), l = 1 cm). (a) UV-vis absorbance spectra. (b) A least square fitting to determine the binding constant K between H**G6** and $\mathbf{1}^{7+}$ (data at λ_{abs} = 290 nm).

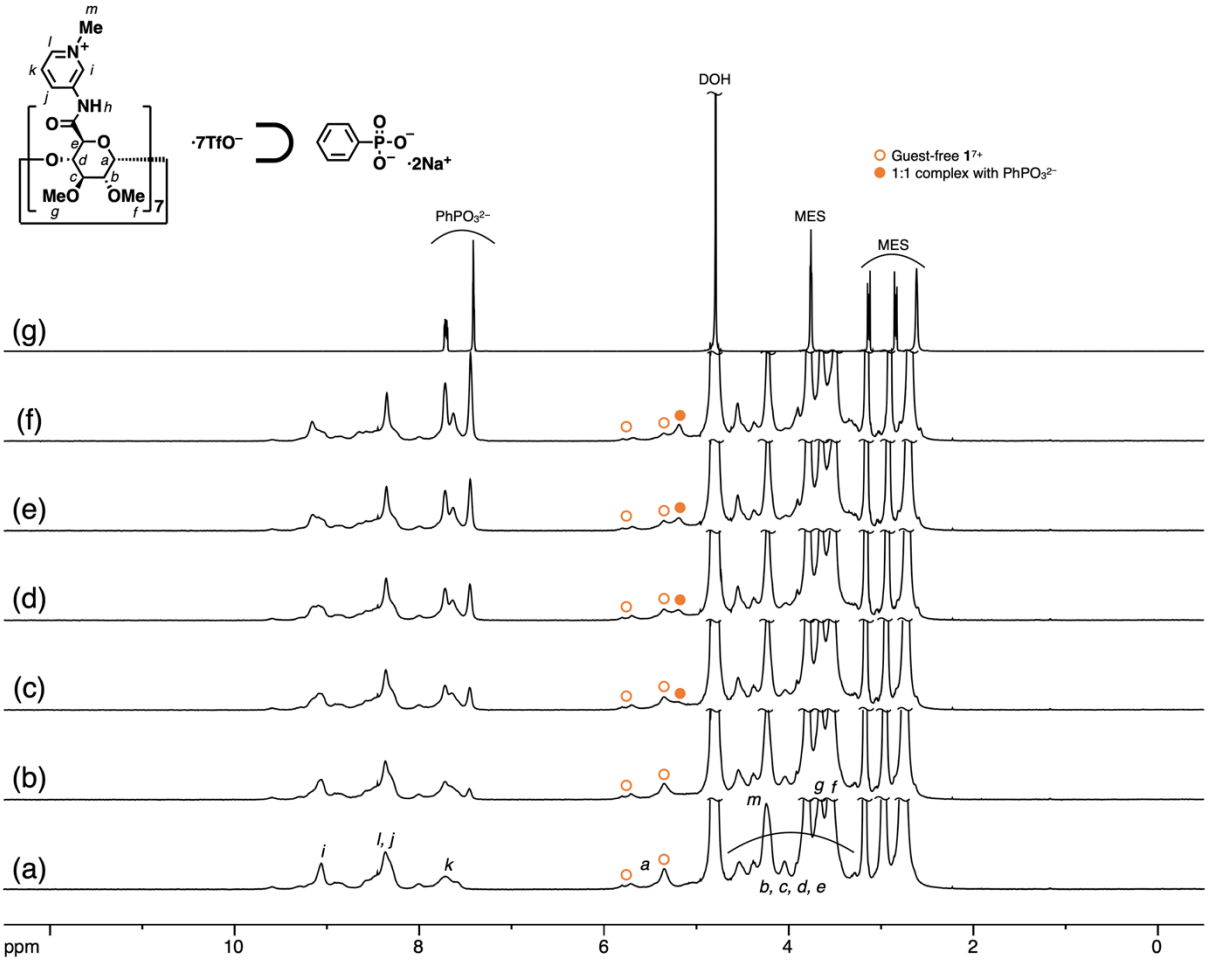

Figure S35. ^{1}H NMR spectra of **1**(OTf)$_7$ and $PhPO_3Na_2$ (**G7**Na_2) (^{1}H NMR, D_2O, [MES buffer] = 32 mM, pH = 7.0 (pD = 7.5), 600 MHz). (a) **1**(OTf)$_7$. (b–f) **1**(OTf)$_7$ + **G7**Na_2. (b) **G7**Na_2 0.5 eq. (c) 1.0 eq. (d) 1.5 eq. (e) 2.0 eq. (f) 3.0 eq. (g) **G7**Na_2.

The binding constant K between **G7**Na_2 and **1**$^{7+}$ was determined from the ^{1}H integral ratio of proton *a*.

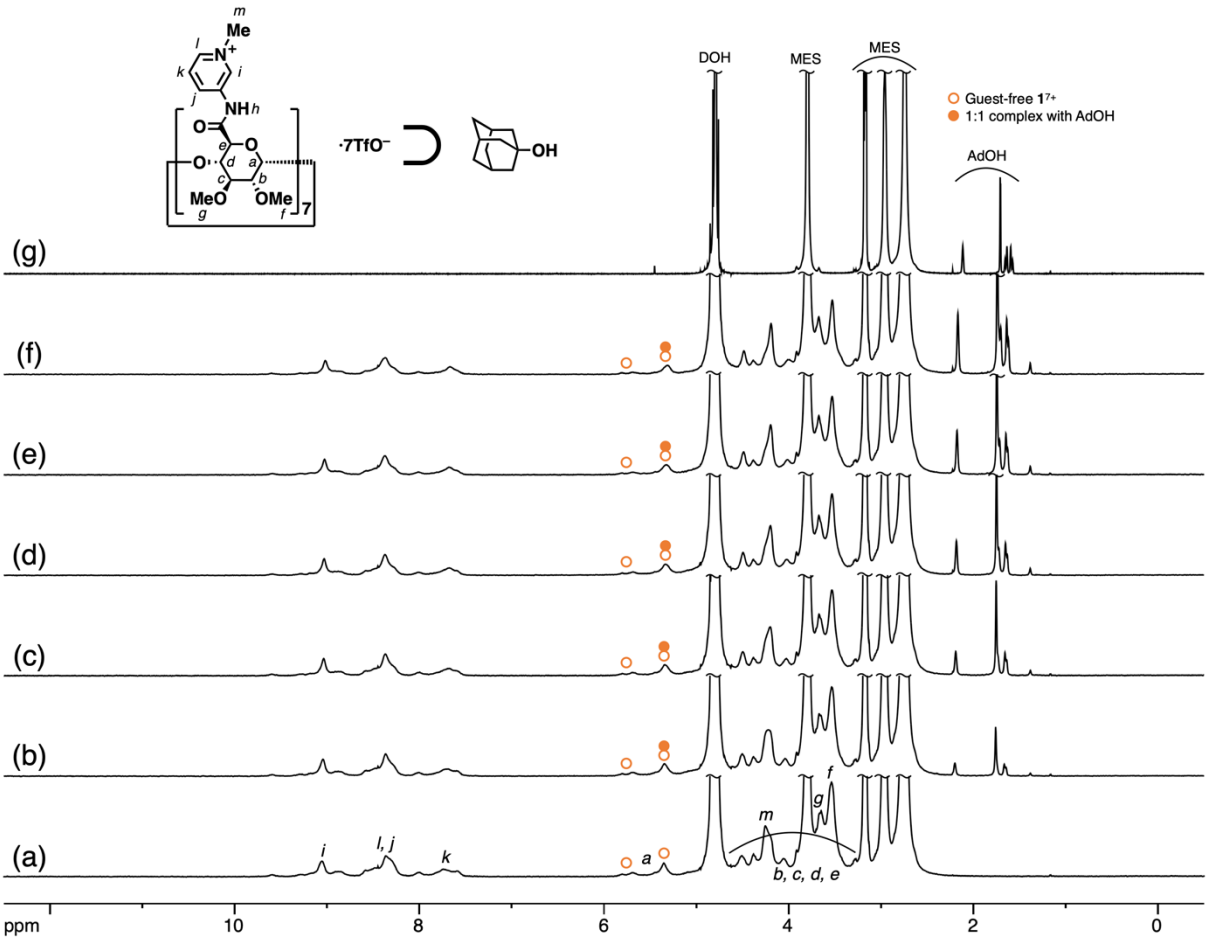

Figure S36. ^{1}H NMR spectra of **1**(OTf)$_7$ and adamantanol **G8** (^{1}H NMR, D_2O, [MES buffer] = 32 mM, pH = 7.0 (pD = 7.5), 600 MHz). (a) **1**(OTf)$_7$. (b–f) **1**(OTf)$_7$ + **G8**. (b) **G8** 0.5 eq. (c) 1.0 eq. (d) 1.5 eq. (e) 2.0 eq. (f) 3.0 eq. (g) **G8**.

The binding constant *K* between **G8** and **1**$^{7+}$ was determined from the ^{1}H integral ratio of proton *a*.

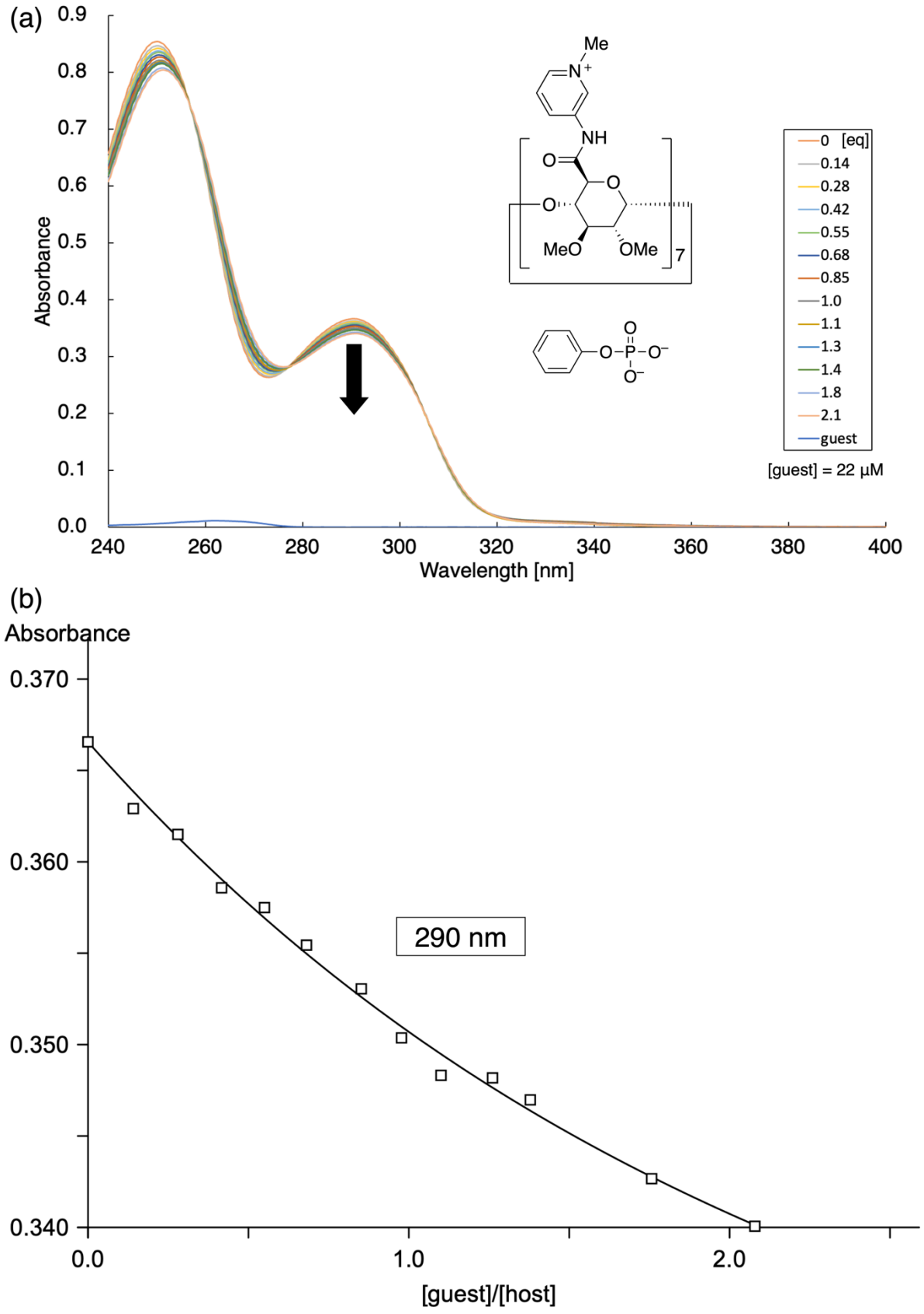

Figure S37. A titration experiment of $PhOPO_3Na_2$ (**G1**Na_2) against **1**$(OTf)_7$ (12 μM) (UV-vis, 0.38 mM MES buffer (pH = 5.5), l = 1 cm). (a) UV-vis absorbance spectra. (b) A least square fitting to determine the binding constant K between **G1**Na_2 and $\mathbf{1}^{7+}$ (data at λ_{abs} = 290 nm).

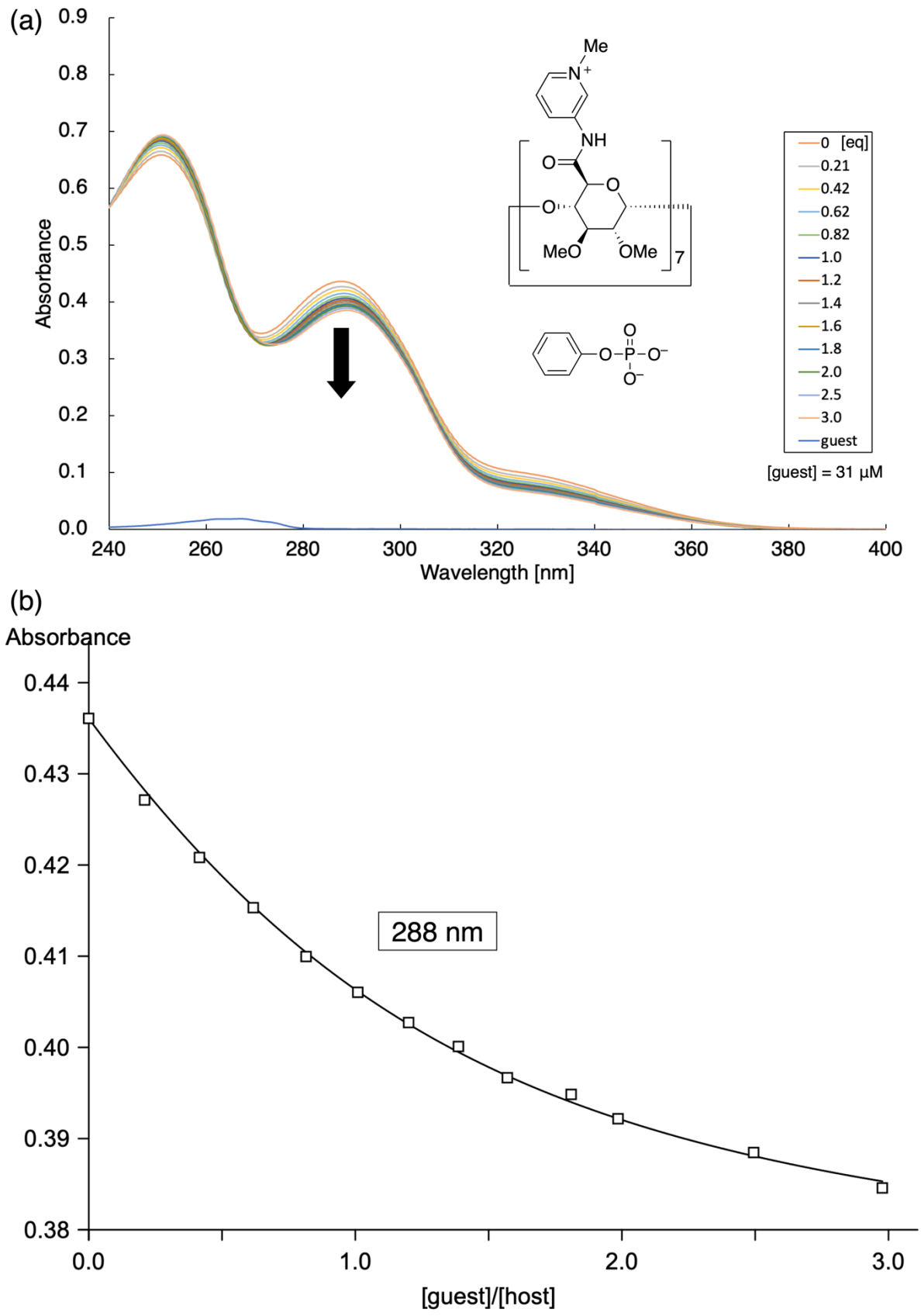

Figure S38. A titration experiment of $PhOPO_3Na_2$ (**G1**Na_2) against **1**$(OTf)_7$ (12 μM) (UV-vis, D_2O, l = 1 cm). (a) UV-vis absorbance spectra. (b) A least square fitting to determine the binding constant K between **G1**Na_2 and $\mathbf{1}^{7+}$ (data at λ_{abs} = 288 nm).

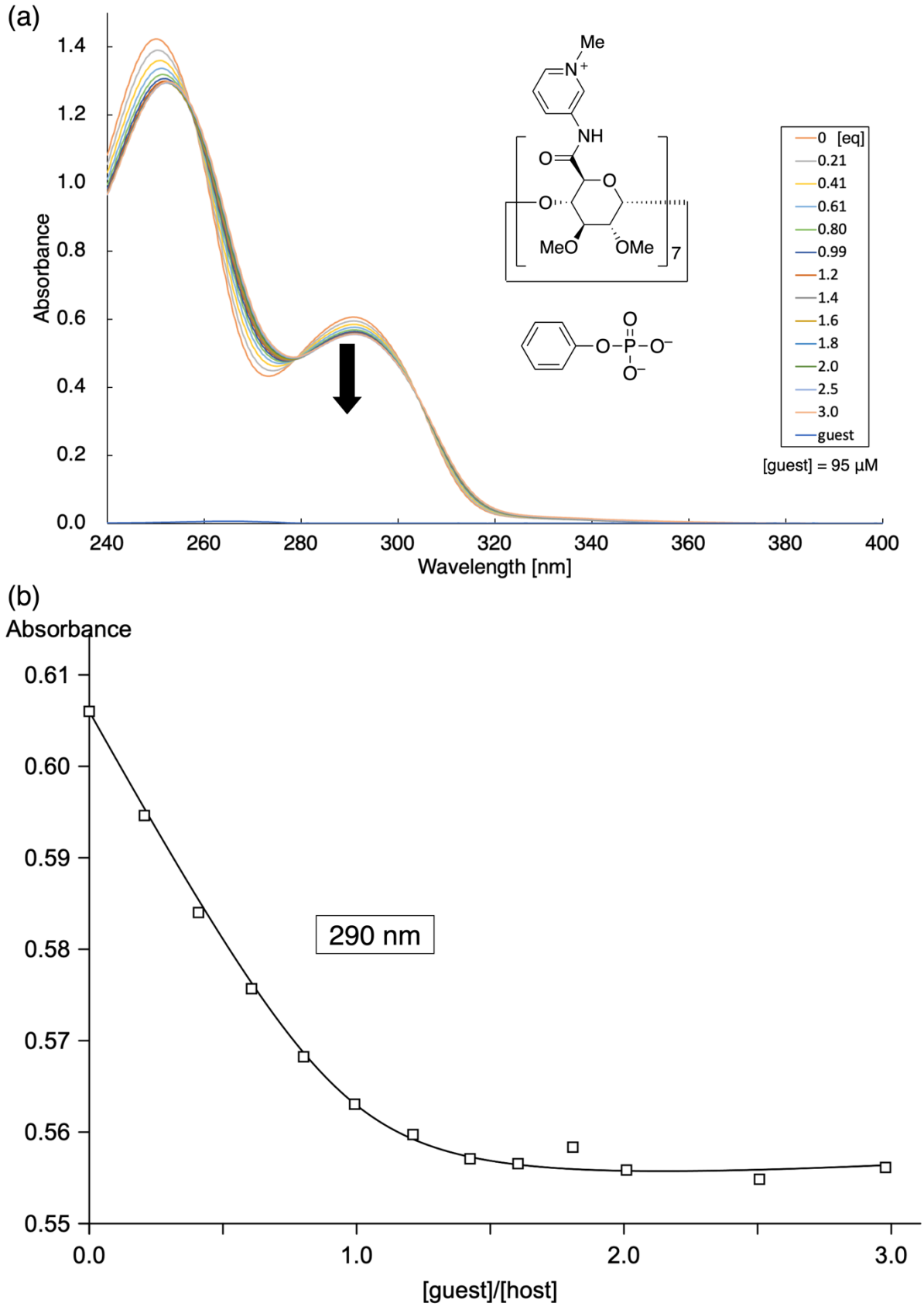

Figure S39. A titration experiment of $PhOPO_3Na_2$ (**G1**Na_2) against **1**$(OTf)_7$ (200 µM) (UV-vis, H_2O, l = 0.1 cm). (a) UV-vis absorbance spectra. (b) A least square fitting to determine the binding constant K between **G1**Na_2 and $\mathbf{1}^{7+}$ (data at λ_{abs} = 290 nm).

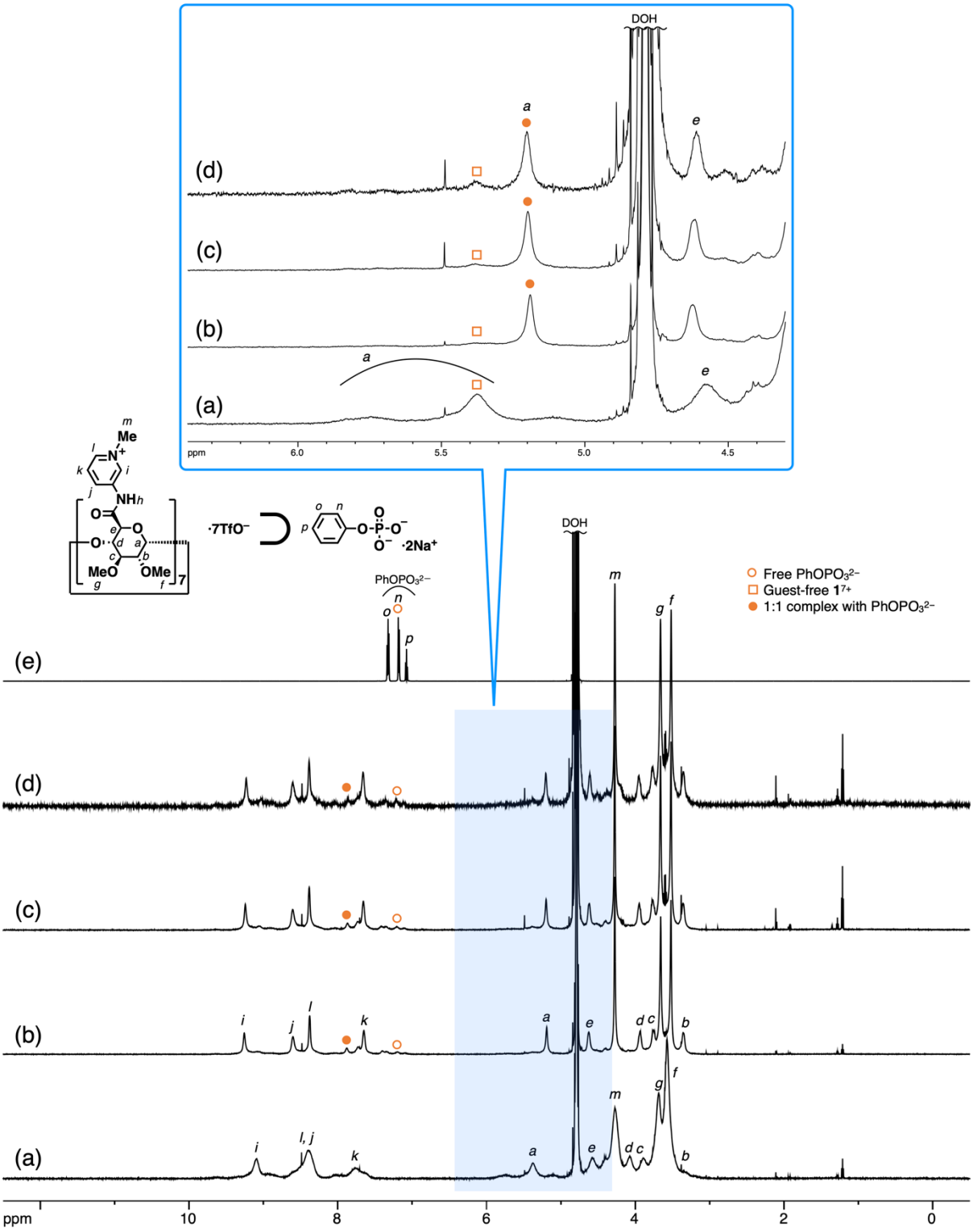

Figure S40. A dilution experiment of 1:1 mixture of **1**(OTf)$_7$ and $PhOPO_3Na_2$ (**G1**Na_2) (^{1}H NMR, 600 MHz, D_2O). (a) **1**(OTf)$_7$ (2.0 mM). (b) **1**(OTf)$_7$ (2.0 mM) + **G1**Na_2 (1.0 eq). (c) **1**(OTf)$_7$ (0.6 mM) + **G1**Na_2 (1.0 eq). (d) **1**(OTf)$_7$ (0.2 mM) + **G1**Na_2 (1.0 eq). (e) **G1**Na_2.

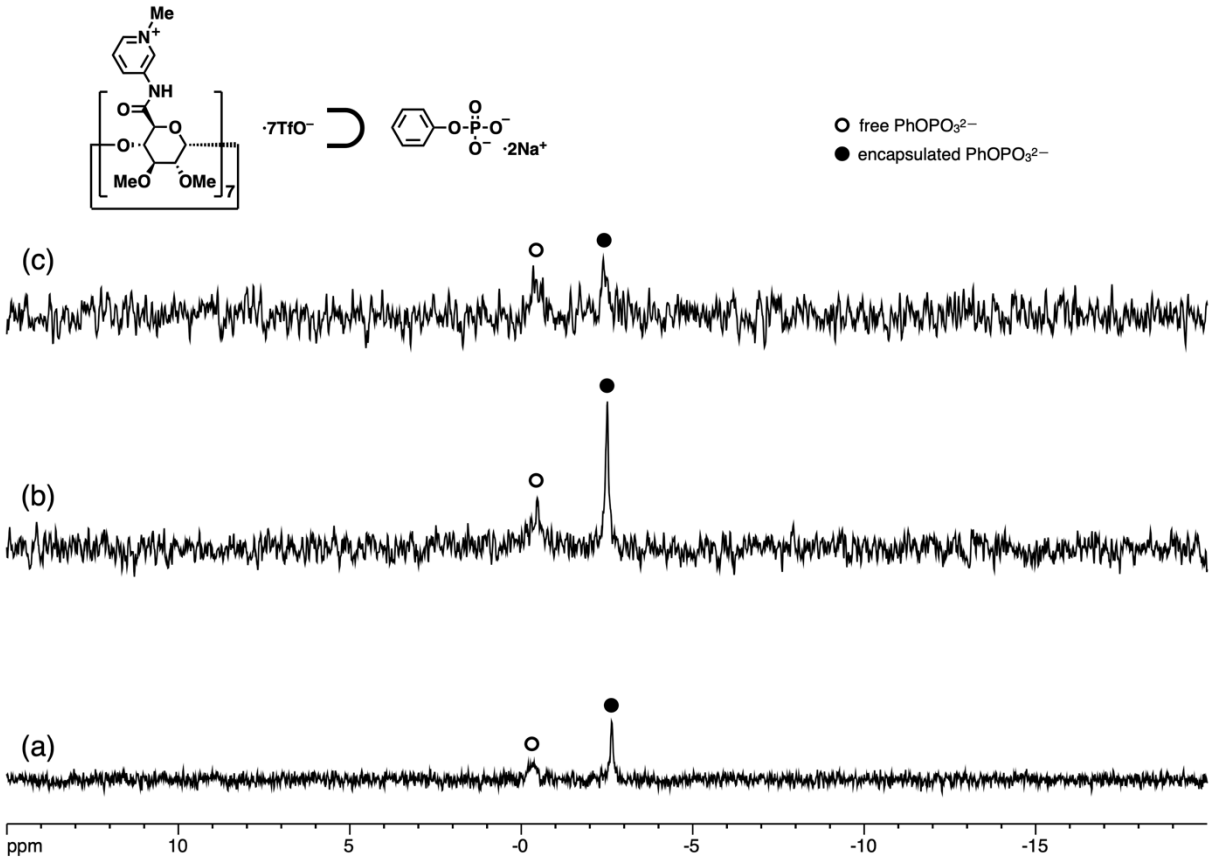

Figure S41. A dilution experiment of 1:1 mixture of **1**$(OTf)_7$ and $PhOPO_3Na_2$ (**G1**Na_2) (^{31}P NMR, 243 MHz, D_2O). (a) **1**$(OTf)_7$ (2.0 mM) + **G1**Na_2 (1.0 eq). (b) **1**$(OTf)_7$ (0.6 mM) + **G1**Na_2 (1.0 eq). (c) **1**$(OTf)_7$ (0.2 mM) + **G1**Na_2 (1.0 eq).

Table S1. Binding constants K [M^{-1}] of **1**$(OTf)_7$ and $PhOPO_3Na_2$ (**G1**Na_2) in various concentration determined from the dilution experiment.

Concentration of **1**$(OTf)_7$ [μM]	log K [M^{-1}] (^1H NMR)	log K [M^{-1}] (^{31}P NMR)
2.0×10^3	3.4	3.2
6.0×10^2	3.9	3.8
2.0×10^2	4.3	4.0

5. Isothermal titration calorimetry

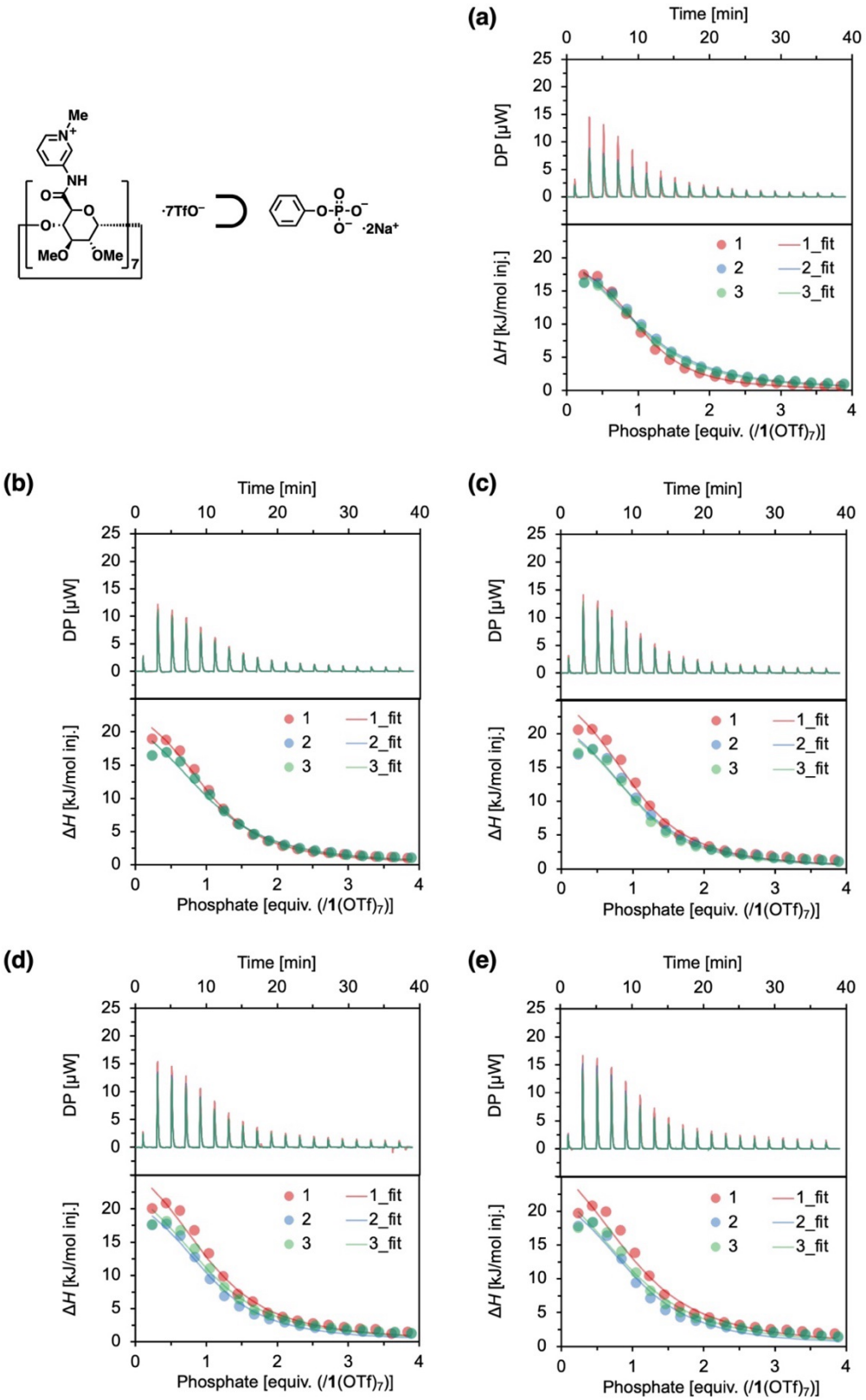

Figure S42. Enthalpograms and Δ*H* change per injection in the ITC experiments of binding of $PhOPO_3Na_2$ (**G1**Na_2) with **1**$(OTf)_7$ in H_2O. Conditions: Cell: **1**$(OTf)_7$, 0.2 mM, 200 μL. Syringe: **G1**Na_2, 4.0 mM. Injection: 2.0 μL each. The data of three independent measurements are presented with curves fitted with a 1:1 binding model. (a) 5 °C. (b) 15 °C. (c) 25 °C. (d) 35 °C. (e) 45 °C.

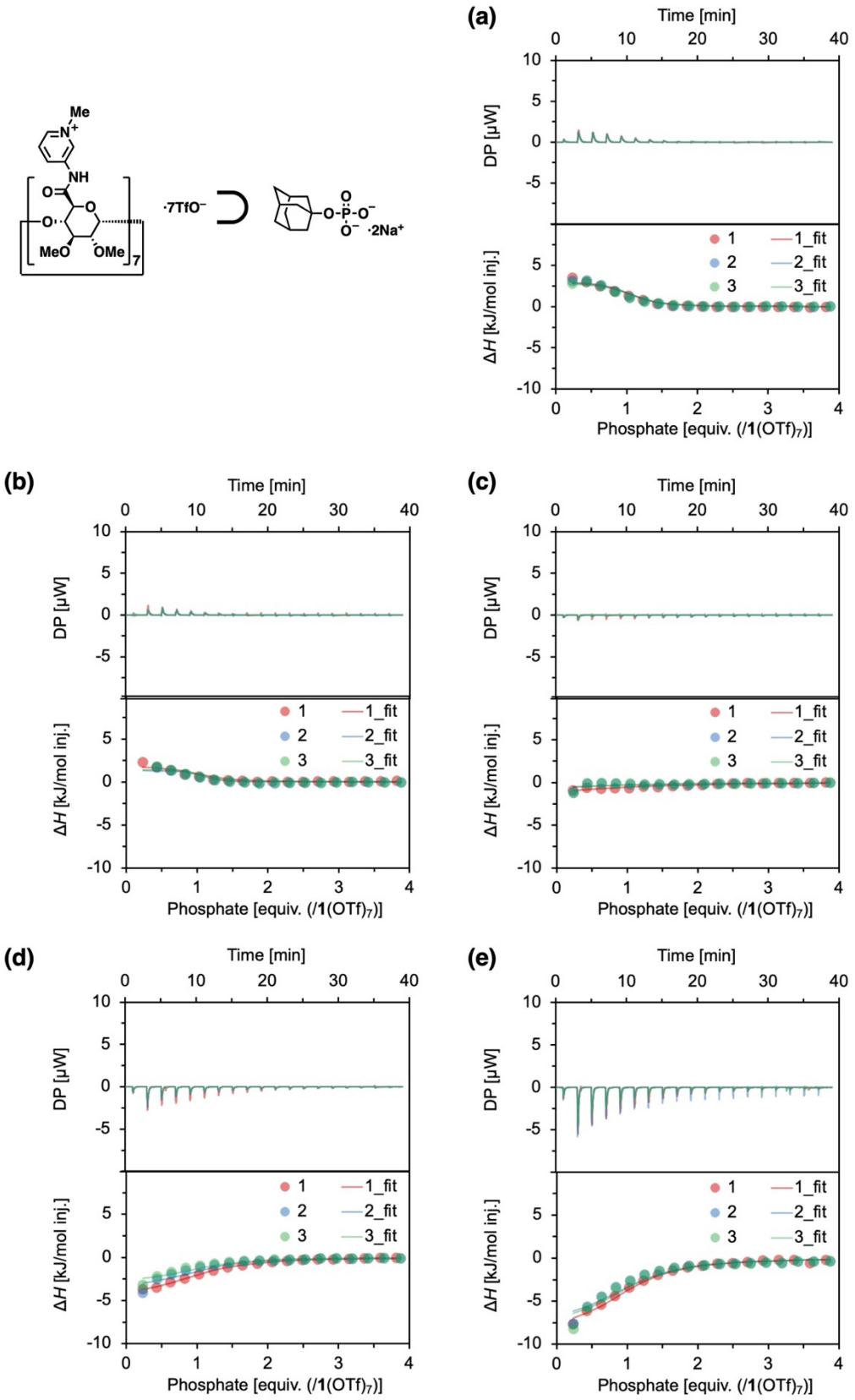

Figure S43. Enthalpograms ΔH change per injection in the ITC experiments of binding of $AdOPO_3Na_2$ (**G2**Na_2) with **1**$(OTf)_7$ in H_2O. Conditions: Cell: **1**$(OTf)_7$, 0.2 mM, 200 μL. Syringe: **G2**Na_2, 4.0 mM. Injection: 2.0 μL each. The data of three independent measurements are presented with curves fitted with a 1:1 binding model. (a) 5 °C. (b) 15 °C. (c) 25 °C. (d) 35 °C. (e) 45 °C.

6. Molecular modeling and simulation

The atomic charges in the host **1**$(OTf)_7$ and the guest molecules ($PhOPO_3^{2-}$, $AdOPO_3^{2-}$, and $PhCO_2^-$) were determined by DFT calculations (HF/6-31G+(d,p) level) using Gaussian 16[S2]. The force-field parameters were assigned within the framework of a second-generation general amber force field (GAFF2)[S9,S10]. The configuration of $\mathbf{1}^{7+}$ was prepared for each host-guest pair, and the counter anions TfO^- were structurally optimized around the inclusion complex. After that, the host-guest distance was continuously enlarged up to 3.8 nm with an interval of 0.025 or 0.100 nm: there are 60 initial configurations for the host-guest structures.

A host-guest structure surrounded by 7 TfO^- was placed at the center of 8 nm cube, which was filled with 18,000 water molecules for TIP4P/Ew.[S11] An MD system thereby consisted of ~72,000 particles including the virtual site employed for the water model. After structural optimization of the system cell, we performed MD simulation for 10 ns under the *NPT* condition with the velocity-rescaling thermostat and Parrinello-Rahman barostat[S12,S13]. Temperature and pressure were 300 K and 1 atm, respectively, and the coupling times of thermostat and barostat were set to 2 ps. The covalent bonds including hydrogen atoms were constrained with the LINCS method[S14]. In the present simulation, the host-guest distance was restrained with the umbrella potential with a force constant of 2,000 kJ/(mol nm^2) and 5,000 kJ/(mol nm^2) for $PhCO_2^-$ and $PhOPO_3^{2-}$/$AdOPO_3^{2-}$, respectively. These equilibration procedures were independently carried out for 30 ns by using all the configurations while changing the host-guest distances. 60 windows in total were used here to run the production MD of 100 ns for the umbrella sampling to quantify a binding free energy of host-guest pairs[S15]: the effective sampling time was totally 6.0 μs. The weighted histogram analysis method with the bootstrap technique[S16] was employed to improve sampling statistics for the potential of mean force.

All the MD calculations were performed by using Gromacs 2016.6 package[S3]. The equations of motion were integrated with the stochastic dynamics at a time step of 2.0 fs. The molecular interactions were evaluated within the framework of GAFF2. The Coulomb interaction was computed with the smooth particle mesh Ewald method with a spline order of 6 and a relative tolerance of 10^{-5} [S17]. The number of reciprocal-scape meshes was set to 96, and the real-space cutoff was 1.4 nm in all the *x*, *y*, *z* directions. The van der Waals interaction was also truncated at 1.4 nm with the switching function for 1.2–1.4 nm.

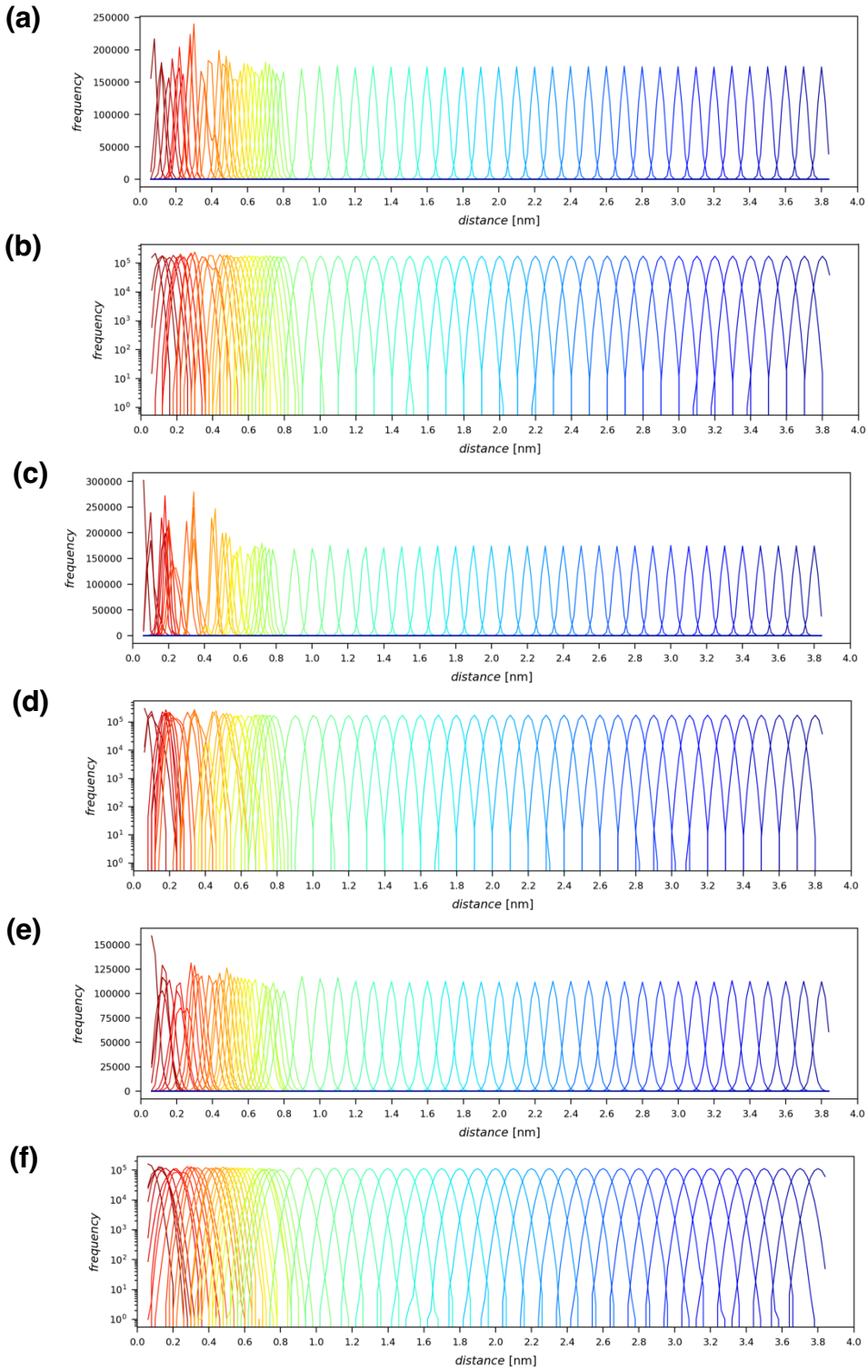

Figure S44. Histogram relationship observed in the reaction coordinate of host-guest inclusion process for the umbrella sampling of MD simulations. The plots in (a,b), (c,d) and (e,f) were obtained in the anion guests of $PhOPO_3^{2-}$, $AdOPO_3^{2-}$ and $PhCO_2^{-}$, respectively. The histograms were displayed within the range of 4.0 nm in the distance between the centers of masses of host and guest molecules. The potentials of mean force shown in Fig. 7b in the main text were computed with this distribution of reaction coordinate.

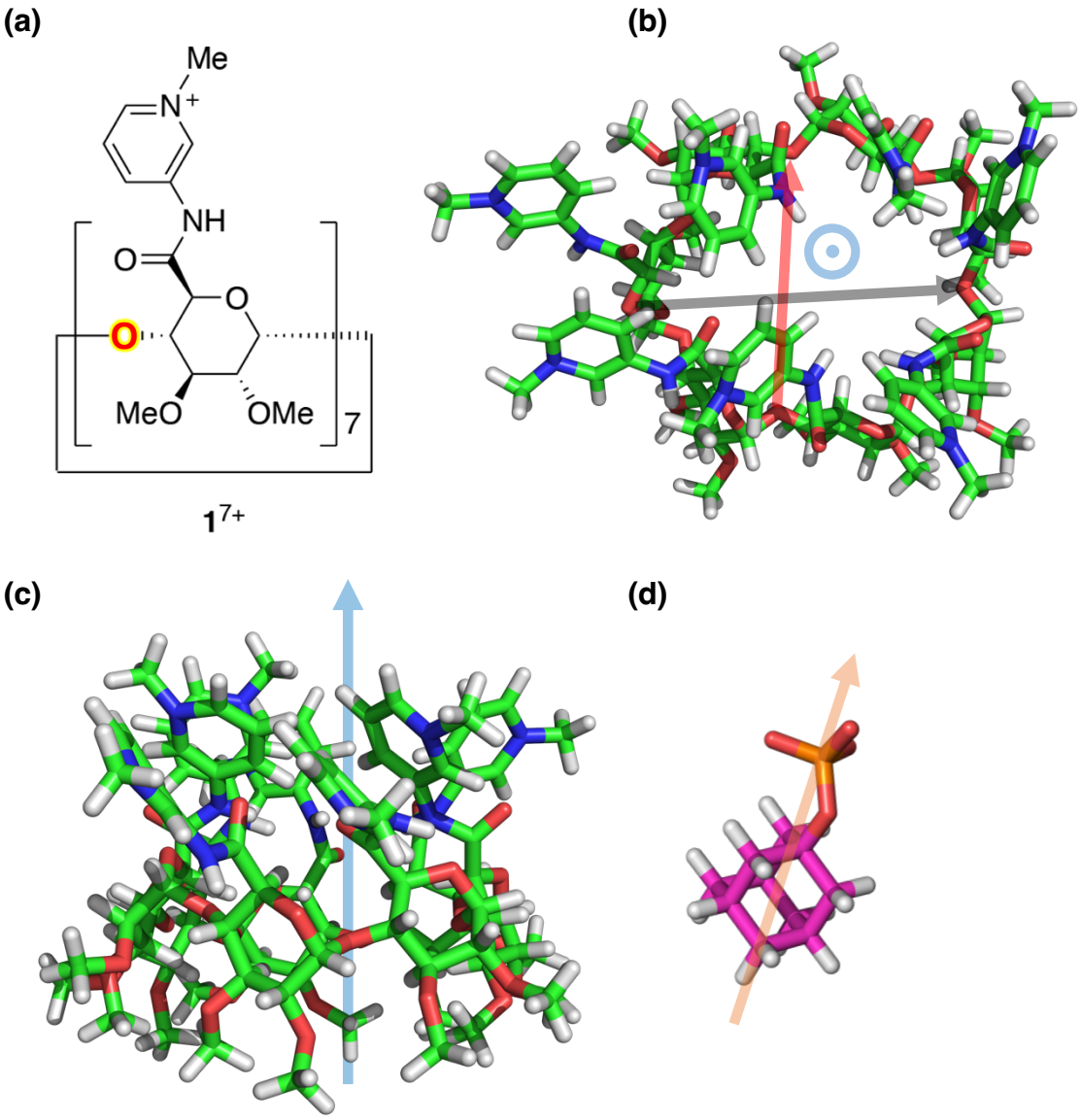

Figure S45. Schematic diagram for the definition of orientation vector and its angle for host and guest molecules. In the cyclodextrin unit of $\mathbf{1}^{7+}$, using the oxygen atom (in red) depicted in (a), the two arrows (in black and red) with the four oxygen atoms were assigned as shown in (b). The orientation vector of $\mathbf{1}^{7+}$ was then defined as an outer product of the tagged two vectors, and the direction of orientation vector was determined toward the pyridinium groups as shown in (c). In the guest molecule, the orientation vector was defined with the two atom centers, the P atom and the farthest C atom as shown in (d). Then, the angle θ was defined with the orientation vectors in (c,d) (in blue and orange). Thereby, in the directions of pyridinium and phosphate groups for host and guest are same in $\cos\theta = 1$, and opposite in $\cos\theta = -1$ in Fig. 7d.

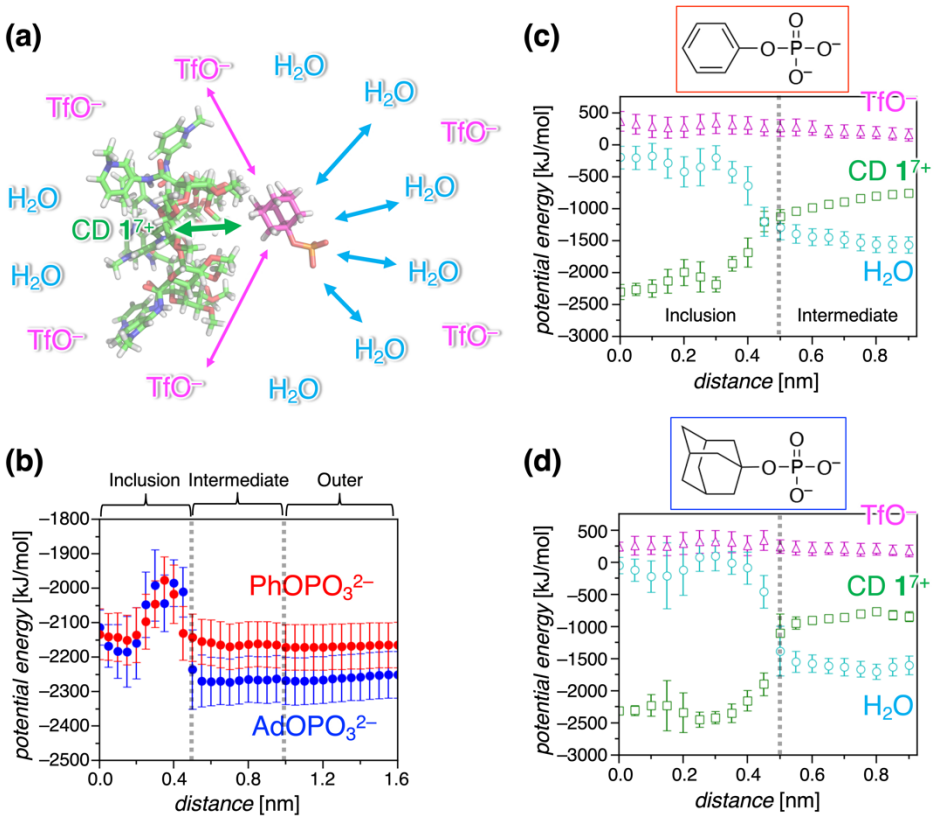

Figure S46. (a) A schematic illustration for the intermolecular interaction of a guest molecule with CD $\mathbf{1}^{7+}$, TfO^- and H_2O molecules in the aqueous solution, and (b–d) energetic profiles of total and partial potential energies of $PhOPO_3^{2-}$ and $AdOPO_3^{2-}$ on the process of binding free energetics in the host-guest interaction of $\mathbf{1}(OTf)_7$. (b) Total potential energy. (c,d) Partial energies of specific solvent species. (c) $PhOPO_3^{2-}$. (d) $AdOPO_3^{2-}$.

Figure S46 shows the schematic illustration and energetic profiles of total and partial potential energies for the phosphate anions with respect to the host-guest distance. The free energy ΔG specified from the calculated PMF (Fig. 7b) consists of the difference in the energetic loss of a guest solute for the formation of the solvation cavity, ΔF, and the difference in the molecular interaction with the surrounding solvent molecules, Δu_{uv} ($\Delta G = \Delta F + \Delta u_{uv}$). The potential energies in Fig. S46b–d correspond to the latter term Δu_{uv}. As seen in Fig. 7d, Fig. S46b–d also indicated that the inclusion profile can be divided into three regions with energy gaps between them; i.e., the outer region (> 1.0 nm), intermediate region (0.5–1.0 nm), and inclusion region (0–0.5 nm). Then, as the guest became included deeper, hydration of the phosphate groups decreased while the interaction with the host CD $\mathbf{1}^{7+}$ increased (Fig. S46c and d). When the anion got closer to the inner cavity (0–0.5 nm, inclusion region), the orientation of the phosphate group reversed to the side of the pyridinium groups of $\mathbf{1}^{7+}$ (Fig. 7c and d). This orientation flip resulted in the loss of the total potential energy (Fig. S46b), particularly as the result of a weakened interaction with the water molecules (Fig. S46c and d). However, in the inclusion region, the energetic disadvantage from the solvation-cavity formation (ΔF included in ΔG) decreased, which leads to an overall stabilization of the binding free energy inside the inner CD cavity (Fig. 7b).

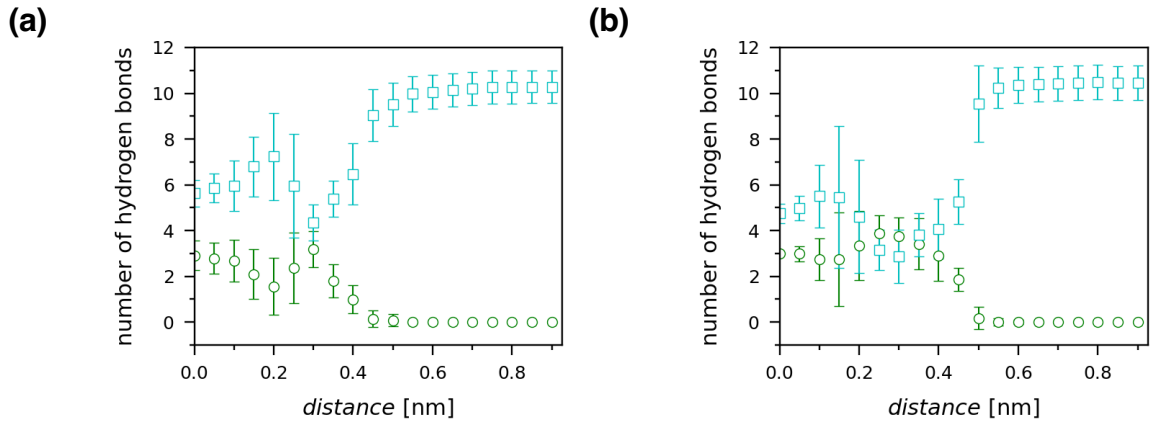

Figure S47. Number of hydrogen bonds of phosphate anions with water (light blue) and $\mathbf{1}^{7+}$ (green). (a) $PhOPO_3^{2-}$. (b) $AdOPO_3^{2-}$.

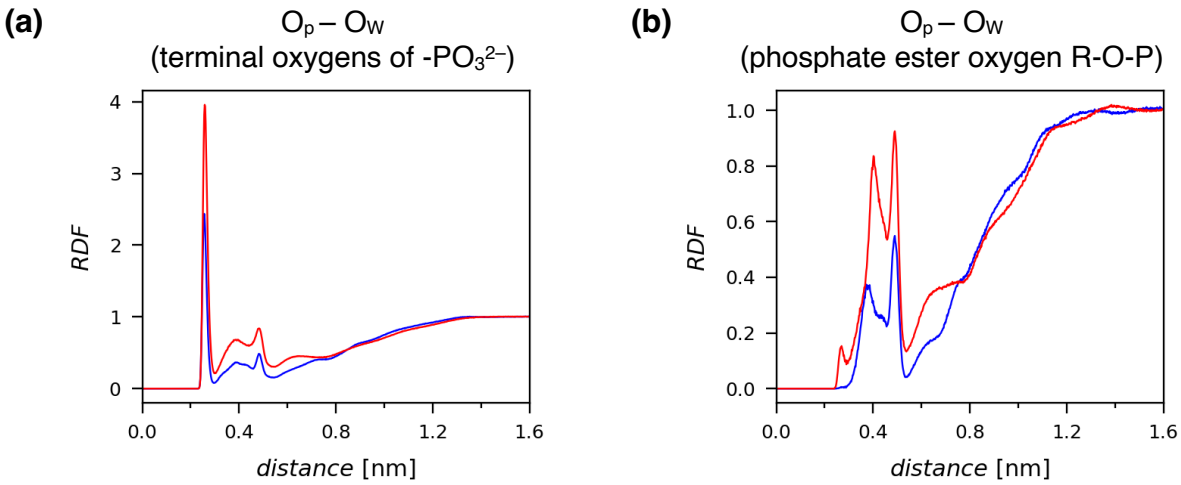

Figure S48. Radial distribution functions between the oxygen atoms of water and phosphate guests. The averaged host-guest distances were 0.212 and 0.097 nm for $PhOPO_3^{2-}$ (red) and $AdOPO_3^{2-}$ (blue) through the MD simulations. The plots in (a) and (b) were obtained for the terminal oxygens of $-PO_3^{2-}$ and the phosphate ester R-O-P, respectively.

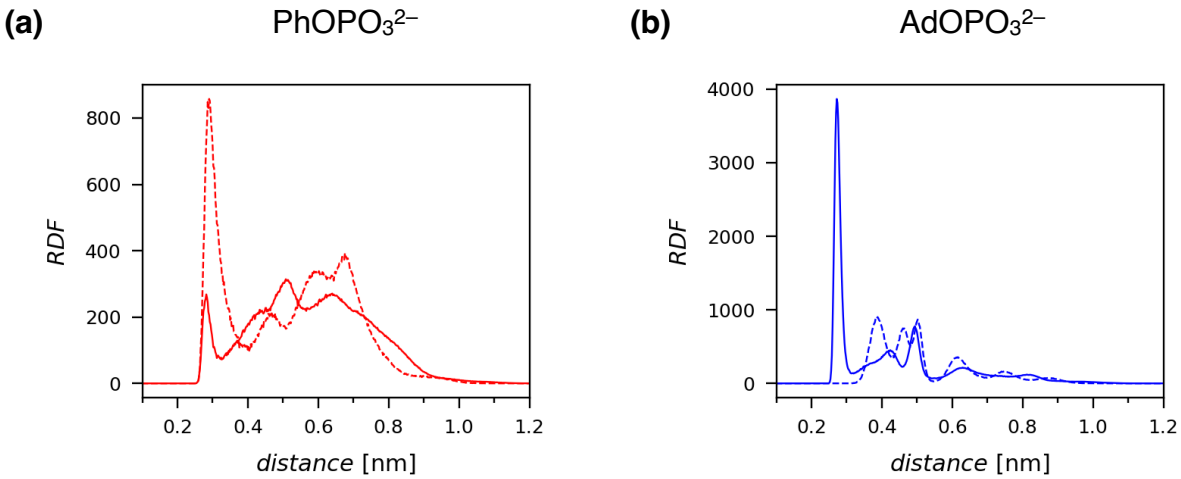

Figure S49. Radial distribution functions between the phosphate oxygen and the amide hydrogen in host $\mathbf{1}^{7+}$. (a) $PhOPO_3^{2-}$. (b) $AdOPO_3^{2-}$. The averaged host-guest distances were 0.212 and 0.097 nm through the MD simulations. The solid line shows the case of the terminal oxygens of $-PO_3^{2-}$, and the dashed line is that of the phosphate ester R-O-P.

The ^{1}H-^{1}H distances between host and guest, $d_{expt.}$(NOE), were determined using the relationship that the integral intensity I in the ^{1}H-^{1}H NOESY NMR signal is inversely proportional to the sixth power of the distance. Intramolecular ^{1}H pairs with a fixed geometry were using it as references, and their values were obtained from the X-ray crystal structure of a similar molecular structure. In this study, the host $\mathbf{1}^{7+}$ and guest phosphates $PhOPO_3^{2-}$/ $AdOPO_3^{2-}$ have multiple equivalent protons, thus the NOE intensities I obtained from the NOESY measurement were normalized according to the number of protons for each correlation.[S18]

Table S2. NOEs intensities (I) of 1:1 complex of $PhOPO_3Na_2$ and $\mathbf{1}(OTf)_7$ and comparison of the distances between proton pairs evaluated from the NOESY measurement ($d_{expt.}$(NOE)) and those obtained by MD simulations ($\langle d_{MD} \rangle$).

Proton pairs	I (obs) [a.u.]	$d_{expt.}$(NOE) [Å]	$\langle d_{MD} \rangle$ [Å]
k–*l*	1.05	2.32[a]	2.48
c–*n*	0.050	3.1	3.47
c–*o*	0.047	3.2	2.93
c–*p*	0.025	3.1	2.77
e–*n*	0.088	2.8	2.61
g–*p*	0.063	3.2	3.04

[*a*] Used as a reference. Value taken from the single-crystal X-ray structure of an *N*-methyl-3-pyridinium amide derivative (CCDC 756624)[S19].

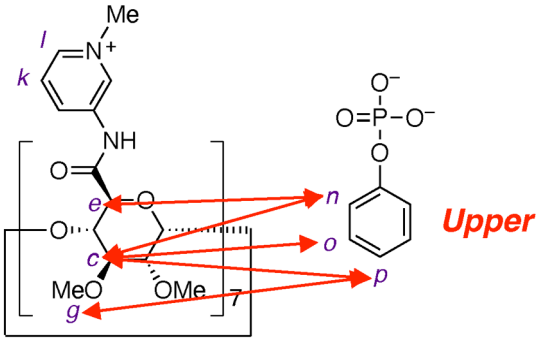

Table S3. NOEs intensities (*I*) of 1:1 complex of $AdOPO_3Na_2$ and **1**$(OTf)_7$ and comparison of the distances between proton pairs evaluated from the NOESY measurement ($d_{expt.}$(NOE)) and those obtained by MD simulations ($\langle d_{MD} \rangle$).

Proton pairs	*I* (obs) [a.u.]	$d_{expt.}$(NOE) [Å]	$\langle d_{MD} \rangle$ [Å]
k–*l*	1.01	2.32[*a*]	2.48
s–*s*′	1.89	1.60[*b*]	1.76
c–*q*	0.311	2.8	2.83
c–*r*	0.181	2.7	2.57
c–*s*	0.116	2.9	2.81
e–*q*	0.477	2.6	2.38
g–*q*	0.261	3.4	3.31
g–*r*	0.327	2.9	3.09
g–*s*	0.272	3.0	3.07
g–*s*′	0.304	3.0	2.95

[*a*] Used as a reference. Value taken from the single-crystal X-ray structure of an *N*-methyl-3-pyridinium amide derivative (CCDC 756624)[S19].

[*b*] Used as a reference. Value taken from the single-crystal X-ray structure of 1-adamantanol (CCDC 971624)[S20].

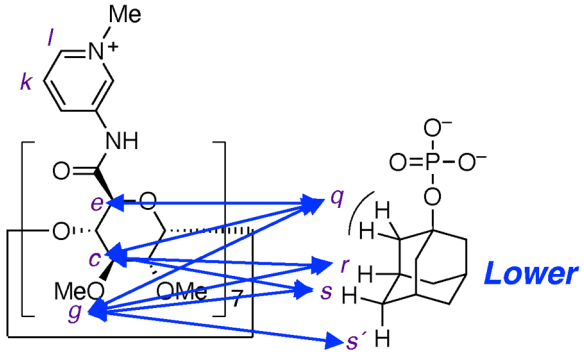

7. References for the supplementary information

S1. G. R. Fulmer, A. J. M. Miller, N. H. Sherden, H. E. Gottlieb, A. Nudelman, B. M. Stoltz, J. E. Bercaw and K. I. Goldberg, *Organometallics*, 2010, **29**, 2176–2179.

S2. M. J. Frisch, G. W. Trucks, H. B. Schlegel, G. E. Scuseria, M. A. Robb, J. R. Cheeseman, G. Scalmani, V. Barone, G. A. Petersson, H. Nakatsuji, X. Li, M. Caricato, A. V. Marenich, J. Bloino, B. G. Janesko, R. Gomperts, B. Mennucci, H. P. Hratchian, J. V. Ortiz, A. F. Izmaylov, J. L. Sonnenberg, D. Williams-Young, F. Ding, F. Lipparini, F. Egidi, J. Goings, B. Peng, A. Petrone, T. Henderson, D. Ranasinghe, V. G. Zakrzewski, J. Gao, N. Rega, G. Zheng, W. Liang, M. Hada, M. Ehara, K. Toyota, R. Fukuda, J. Hasegawa, M. Ishida, T. Nakajima, Y. Honda, O. Kitao, H. Nakai, T. Vreven, K. Throssell, J. A. Montgomery, Jr., J. E. Peralta, F. Ogliaro, M. J. Bearpark, J. J. Heyd, E. N. Brothers, K. N. Kudin, V. N. Staroverov, T. A. Keith, R. Kobayashi, J. Normand, K. Raghavachari, A. P. Rendell, J. C. Burant, S. S. Iyengar, J. Tomasi, M. Cossi, J. M. Millam, M. Klene, C. Adamo, R. Cammi, J. W. Ochterski, R. L. Martin, K. Morokuma, O. Farkas, J. B. Foresman and D. J. Fox, Gaussian 16, Revision C.01, Gaussian, Inc., Wallingford, CT, USA, 2016.

S3. M. J. Abraham, T. Murtola, R. Schulz, S. Páll, J. C. Smith, B. Hess and E. Lindahl, *SoftwareX*, 2015, **1–2**, 19–25.

S4. T. Kraus, M. Buděšínský and J. Závada, *Eur. J. Org. Chem.*, 2000, 3133–3137.

S5. T. Nakamura, S. Yonemura and T. Nabeshima, *Chem. Commun.*, 2019, **55**, 3872–3875.

S6. L. Jullien, J. Canceill, L. Lacombe and J.-M. Lehn, *J. Chem. Soc., Perkin Trans. 2*, 1994, 989–1002.

S7. V. V. Nemmara, D. F. Xiang, A. A. Fedorov, E. V. Fedorov, J. B. Bonanno, S. C. Almo and F. M. Raushel, *Biochemistry*, 2018, **57**, 6219–6227.

S8. M. V. Anokhin, N. V. Averina, N. V. Zyk and O. N. Zefirova, *Moscow Univ. Chem. Bull.*, 2008, **49**, 241–245.

S9. J. Wang, R. M. Wolf, J. W. Caldwell, P. A. Kollman and D. A. Case, *J. Comput. Chem.*, 2004, **25**, 1157–1174.

S10. D. A. Case, I. Y. Ben-Shalom, S. R. Brozell, D. S. Cerutti, T. E. Cheatham, III, V. W. D. Cruzeiro, T. A. Darden, R. E. Duke, D. Ghoreishi, G. Giambasu, T. Giese, M. K. Gilson, H. Gohlke, A. W. Goetz, D. Greene, R. Harris, N. Homeyer, Y. Huang, S. Izadi, A. Kovalenko, R. Krasny, T. Kurtzman, T. S. Lee, S. Le Grand, P. Li, C. Lin, J. Liu, T. Luchko, R. Luo, V. Man, D. J. Mermelstein, K. M. Merz, Y. Miao, G. Monard, C. Nguyen, H. Nguyen, A. Onufriev, F. Pan, R. Qi, D. R. Roe, A. Roitberg, C. Sagui, S. Schott-Verdugo, J. Shen, C. L. Simmerling, J. Smith, J. Swails, R. C. Walker, J. Wang, H. Wei, L. Wilson, R. M. Wolf, X. Wu, L. Xiao, Y. Xiong, D. M. York and P. A. Kollman, AMBER 2019/Amber-Tools19, University of California, San Francisco, CA, USA, 2019.

S11. H. W. Horn, W. C. Swope, J. W. Pitera, J. D. Madura, T. J. Dick, G. L. Hura and T. Head-Gordon, *J. Chem. Phys.*, 2004, **120**, 9665–9678.

S12. G. Bussi, D. Donadio and M. Parrinello, *J. Chem. Phys.*, 2007, **126**, 014101.

S13. M. Parrinello and A. Rahman, *J. Appl. Phys.*, 1981, **52**, 7182–7190.

S14. B. Hess, H. Bekker, H. J. C. Berendsen and J. G. E. M. Fraaije, *J. Comput. Chem.*, 1997, **18**, 1463–1472.

S15. W. You, Z. Tang and C. E. A. Chang, *J. Chem. Theory Comput.*, 2019, **15**, 2433–2443.

S16. J. S. Hub, B. L. de Groot and D. van der Spoel, *J. Chem. Theory Comput.*, 2010, **6**, 3713–3720.

S17. U. Essmann, L. Perera, M. L. Berkowitz, T. Darden, H. Lee and L. G. Pedersen, *J. Chem. Phys.*, 1995, **103**, 8577–8593.

S18. J. S. Mugridge, A. Zahl, R. van Eldik, R. G. Bergman and K. N. Raymond, *J. Am. Chem. Soc.*, 2013, **135**, 4299–4306.

S19. A. Dorazco-González, H. Höpfl, F. Medrano and A. K. Yatsimirsky, *J. Org. Chem.*, 2010, **75**, 2259–2273.
S20. J. G. Garcia and F. R. Fronczek, CCDC 971624: Experimental Crystal Structure Determination, 2014.